Radiative outputs of blazars
(radiative processes, escape, light crossing, Klain-Nishina effects, synchrotron bump)

Rafał MODERSKI
Nicolaus Copernicus Astronomical Center

OUTLINE

1. General picture
    a. magnetic field, beaming patterns
2. "Shock in a jet" model
    a. flares, lags
3. Bulk Compton radiation
    a. jet content
4. Klein-Nishina effects
5. Summary

BASIC MODEL

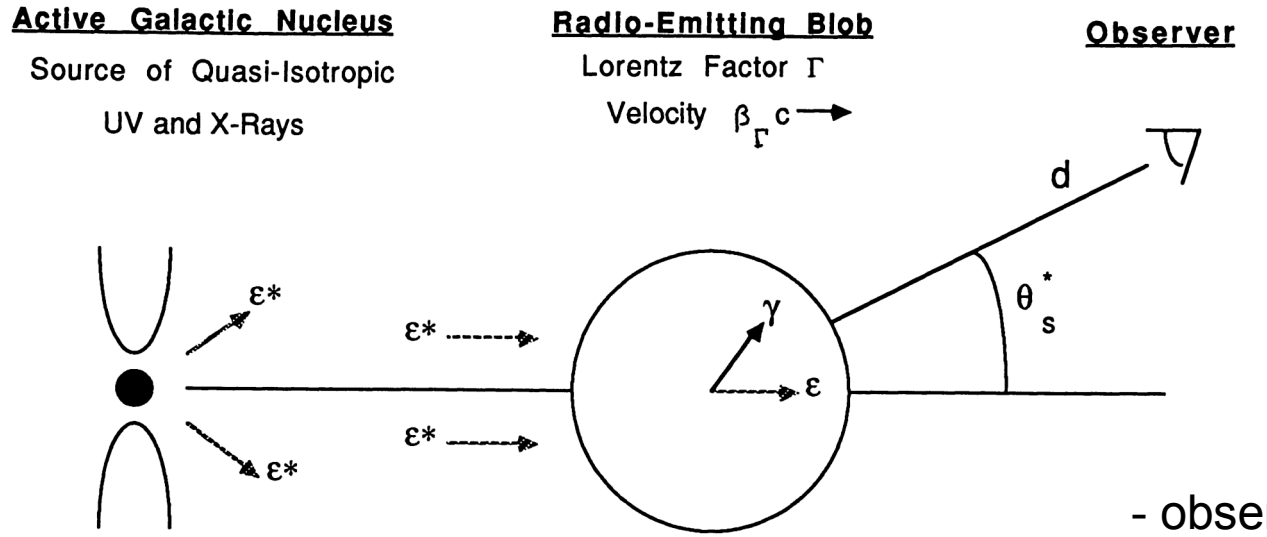

- direct disc radiation and reprocessed disc radiation
- radiation is usually monochromatic

- blob has a size R~r Θj
- usually Θj is 1/Γ
- electrons within the blob have a distribution n(γ)
-these electrons emit synchrotron radiation and comptonize both external and internal photon fields

- observer is located at Θobs = Θj, so at the edge of the jet

BASIC MODEL

SSC vs. ERC model

- assume a blazar with two spectral components F_{syn} i F_γ and compare u'_B i u'_γ

- in SSC model

$$q = \frac{F_\gamma}{F_{syn}} = \frac{u'_{SSC}}{u'_{syn}} = A$$

$$\frac{u'_B}{u'_\gamma} = \frac{u'_B}{u'_{syn}} \frac{u'_{syn}}{u'_{SSC}} = \frac{1}{A^2} = \frac{1}{q^2}$$

- in ERC model

$$q = \frac{F_\gamma}{F_{syn}} = \frac{f\, u'_{EC}}{u'_{syn}}$$

$$\frac{u'_B}{u'_\gamma} = \frac{u'_{syn}/A}{u'_{EC}} = \frac{f}{Aq}$$

where $f \sim (D/\Gamma)^2$ accounts for anisotropy of IC radiation in the source co-moving frame

Hence, in SSC models $q \gg 1$ is possible only for $u'_B \ll u'_\gamma$, while EC can give $q \gg 1$ even for $u'_B > u'_\gamma$, provided $A < f/q$ (same for u'_B and u'_e).

"SHOCK IN A JET" SCENARIO

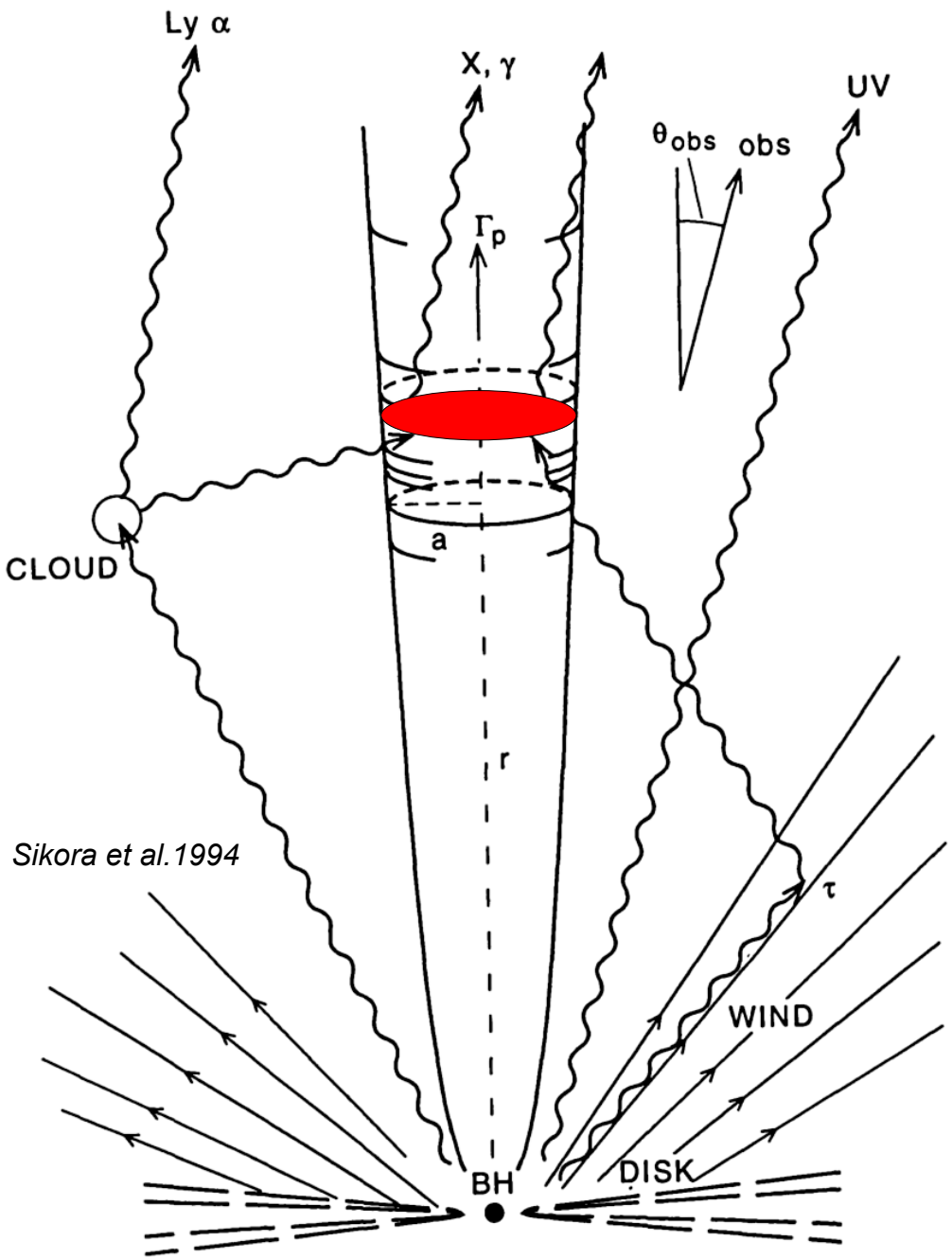

Sikora et al.1994

- shell is assumed to be thin (space between forward and reverse shock formed during collision)

$$\frac{\lambda'}{a} = (\beta_f + \beta_r)\frac{\Delta r_{coll}}{r}$$

- cone geometry of the jet and observer located at Θobs (time delays and different beaming)

- jet has an opening angle 1/Γ (for narrow jet SSC problem, for wide jet energy requirement problem)

NON-THERMAL FLARES IN BLAZARS

Electron evolution

Sikora et al. 2001

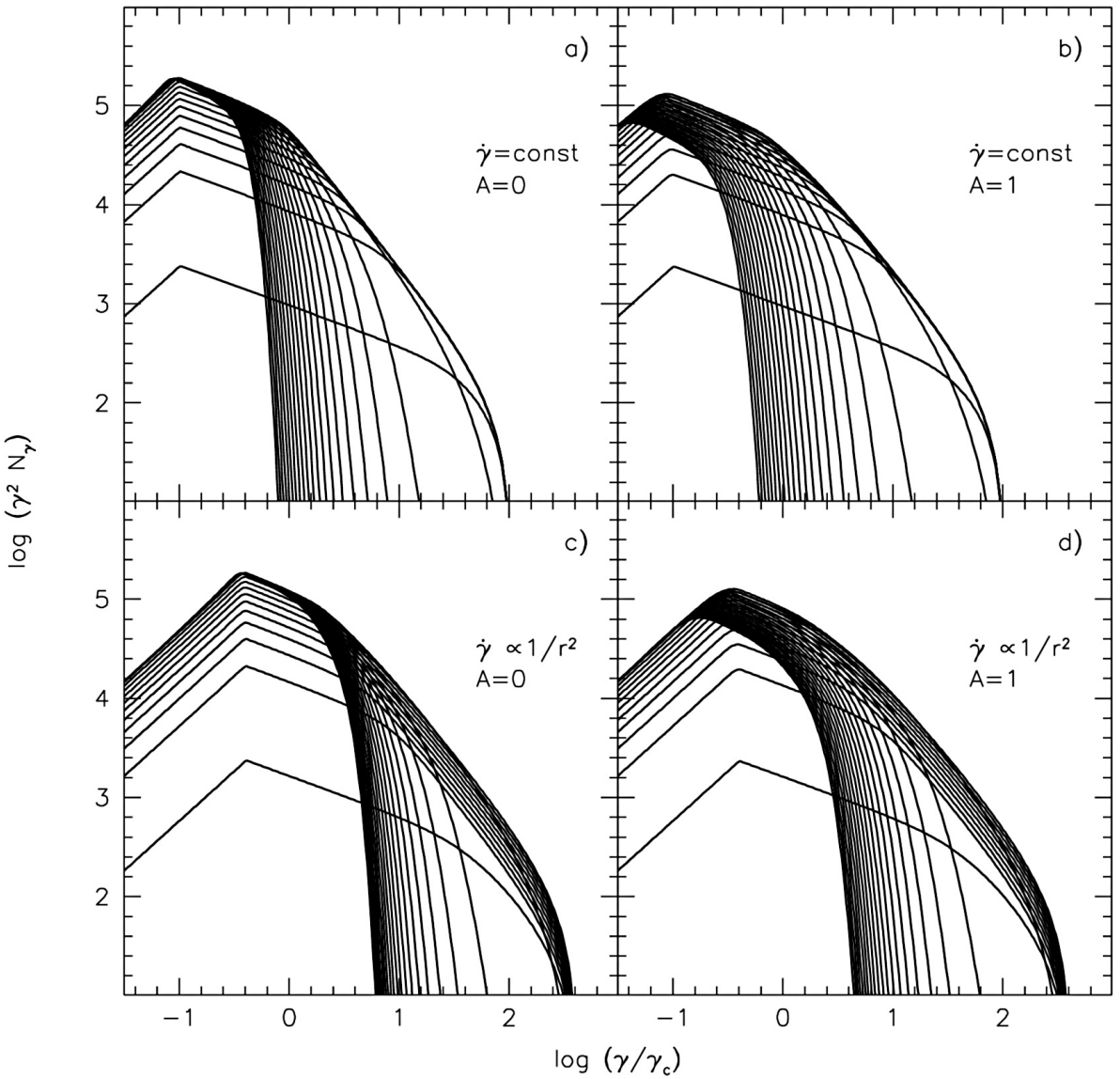

- electrons accelerated and injected into the shell ($t_{acc} << t_{inj}$) according to $Q \sim \gamma^{-p}$

- the electrons evolve

$$\frac{\partial N_\gamma}{\partial t} = \frac{\partial}{\partial \gamma}\left(\dot{\gamma} N_\gamma\right) + Q$$

- radiative cooling timescale

$$t_{cool} = \frac{\gamma}{\dot{\gamma}} \Gamma$$

- cooling break

$$\dot{\gamma} = b \gamma^2$$

$$\gamma_c = \frac{\Gamma c}{b \Delta r_{inj}}$$

- fast cooling vs slow cooling

Electron distribution is shaped by the interplay between t_{acc}, t_{inj} and t_{cool}.

NON-THERMAL FLARES IN BLAZARS

Flare shape

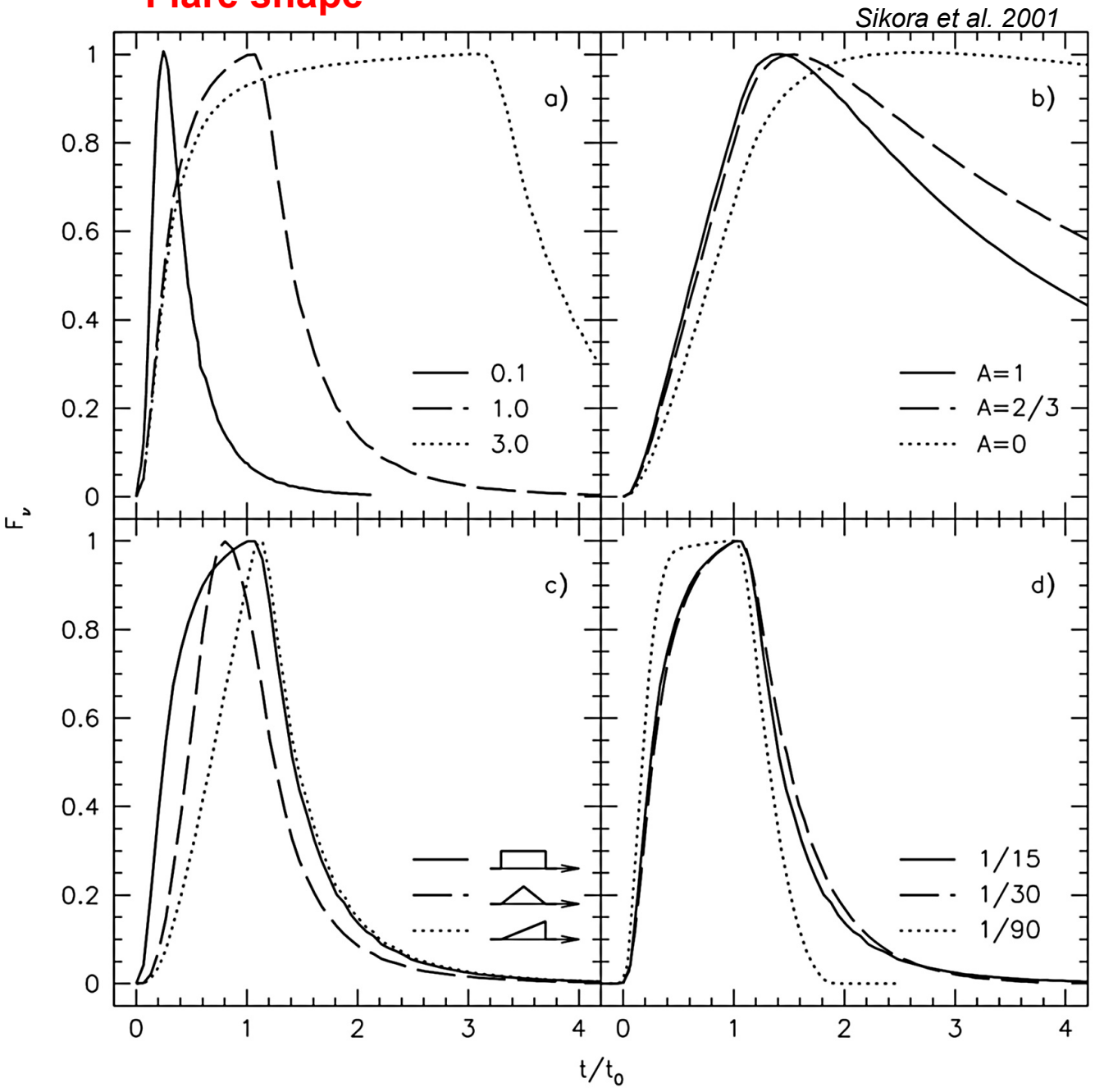

- symmetric flares for Δr_{inj} similar to r

- flares produced in slow cooling regime have very long decay times

- weak dependence on injection profile due to transverse size time delay effects

FIG. 2. Flare profiles : (a) for different values of the injection distance range (b) for different adiabaticities, (c) for different electron injection time profiles, (d) for different jet opening angles

NON-THERMAL FLARES IN BLAZARS

Frequency dependent lags

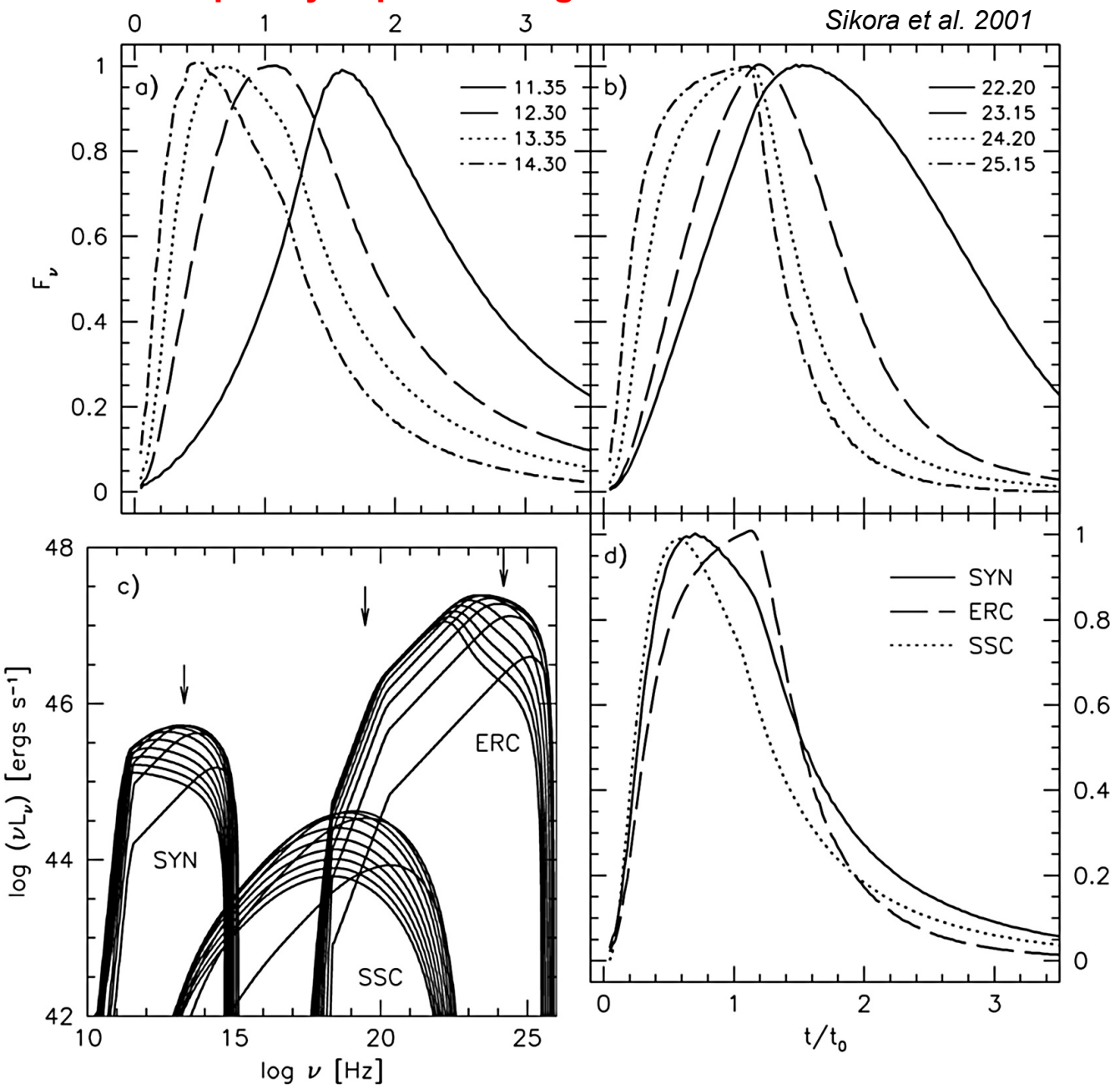

- for synchrotron component lag is significant due to decaying magnetic field ($\nu_{syn} \sim \Gamma\gamma^2 B'$)

- effect is less pronounced for ERC component because ν_{ext} is constant ($\nu_{ERC} \sim \Gamma^2\gamma^2\nu_{ext}$)

- decaying magnetic field also causes synchrotron flare to peak earlier than ERC flare

NON-THERMAL FLARES IN BLAZARS

Simultaneous flares

Wehrle et al. 1998

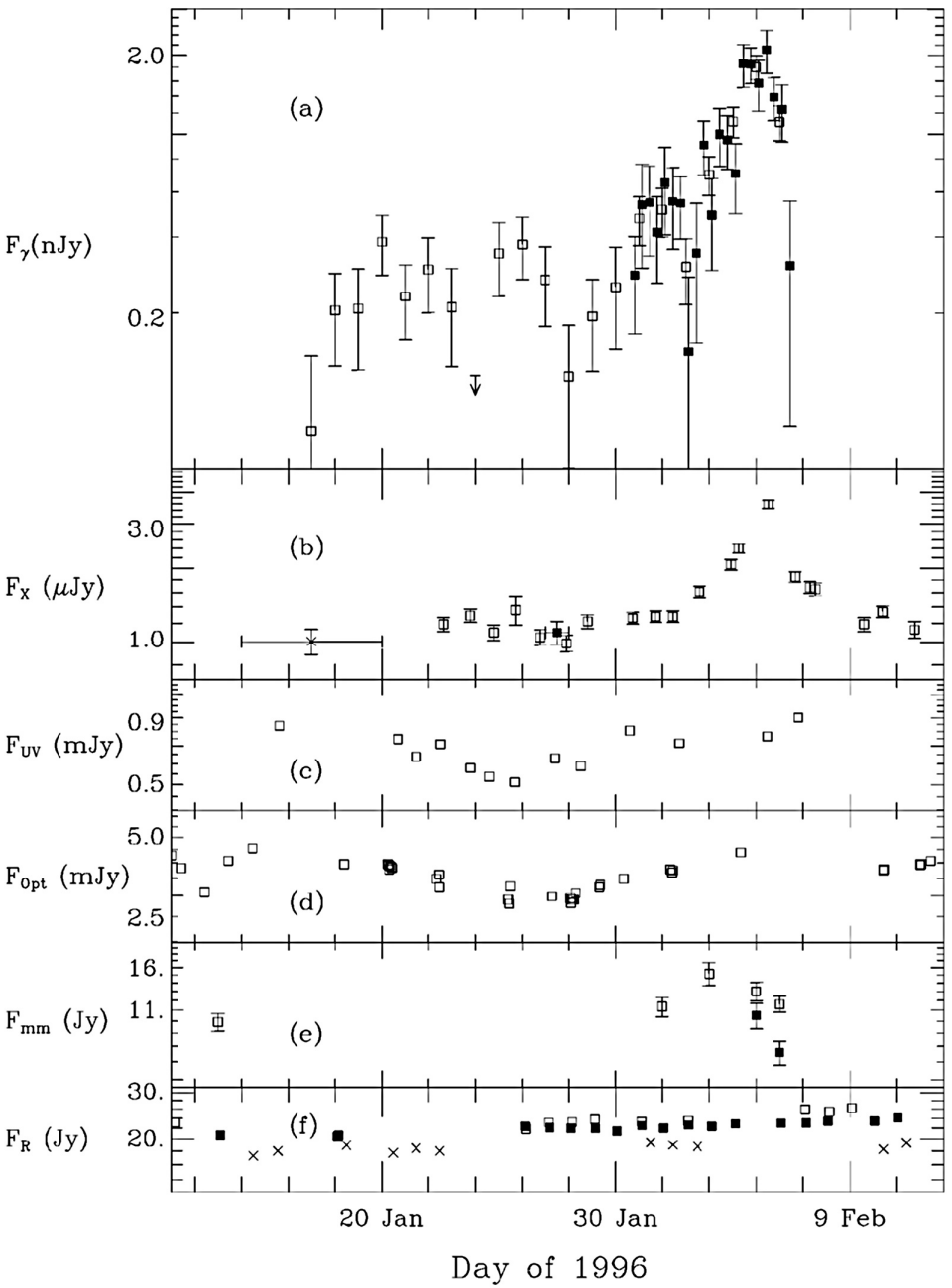

- no time lags between X-rays and γ-rays and similar flare profiles – significant contribution of SSC
- strong dilution required in optical band – most radiation produced elsewhere

Moderski et al. 2003

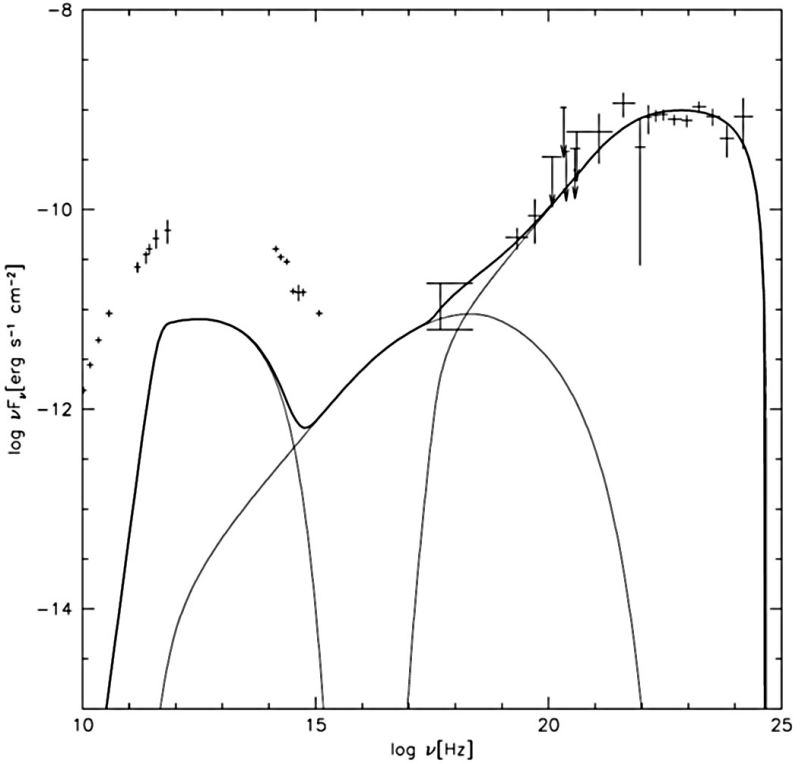

Fig. 2. The average spectrum of the blazar 3C 279 during the February 1996 flare. Data points are from Hartman et al. (2001). Thick, solid line shows the averaged spectrum of our model (see text for parameters). Thin lines represent various components of the spectrum.

NON-THERMAL FLARES IN BLAZARS

Orphan flares

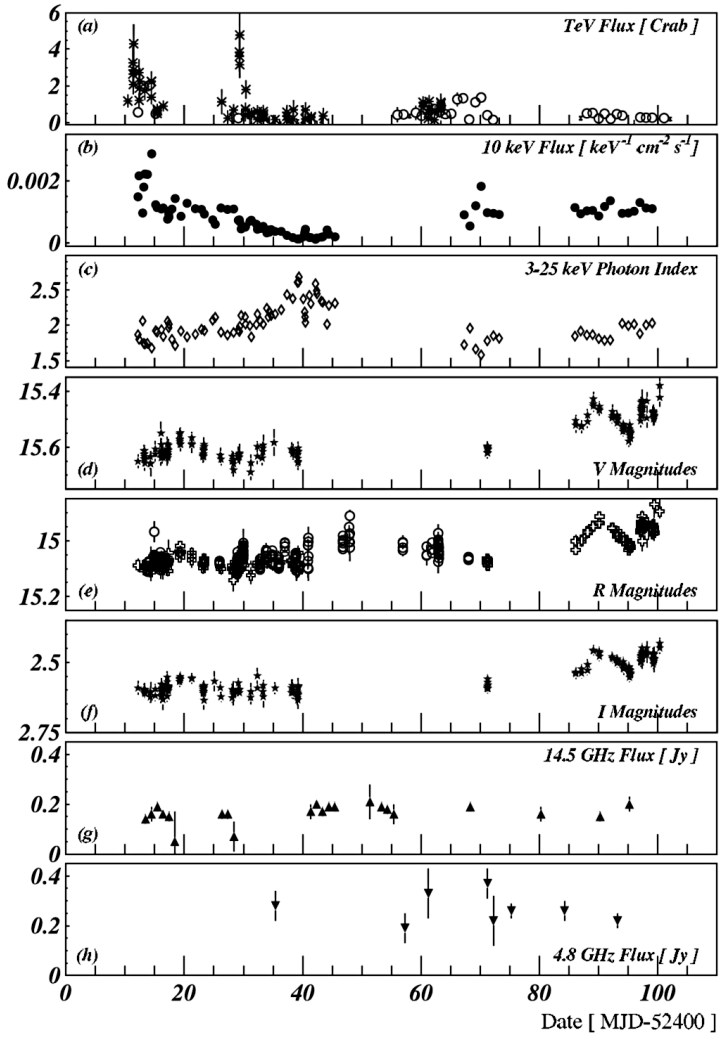

FIG. 2.—Results from the 1ES 1959+650 multiwavelength campaign (2002 May 16–August 14). (*a*) Whipple (*stars*) and HEGRA (*circles*) integral TeV γ-ray fluxes in Crab units above 600 GeV and 2 TeV, respectively; the Whipple data are binned in 20 minute bins and the HEGRA data in diurnal bins. (*b*) *RXTE* X-ray flux at 10 keV. (*c*) *RXTE* 3–25 keV X-ray photon index. (*d*) Absolute *V* magnitudes (Boltwood). (*e*) Absolute *R* magnitudes (*crosses*: Boltwood; *circles*: Abastumani). (*f*) Relative *I* magnitudes (Boltwood); (*g*) The 14.5 GHz flux density (UMRAO). (*h*) The 4.8 GHz flux density (UMRAO).

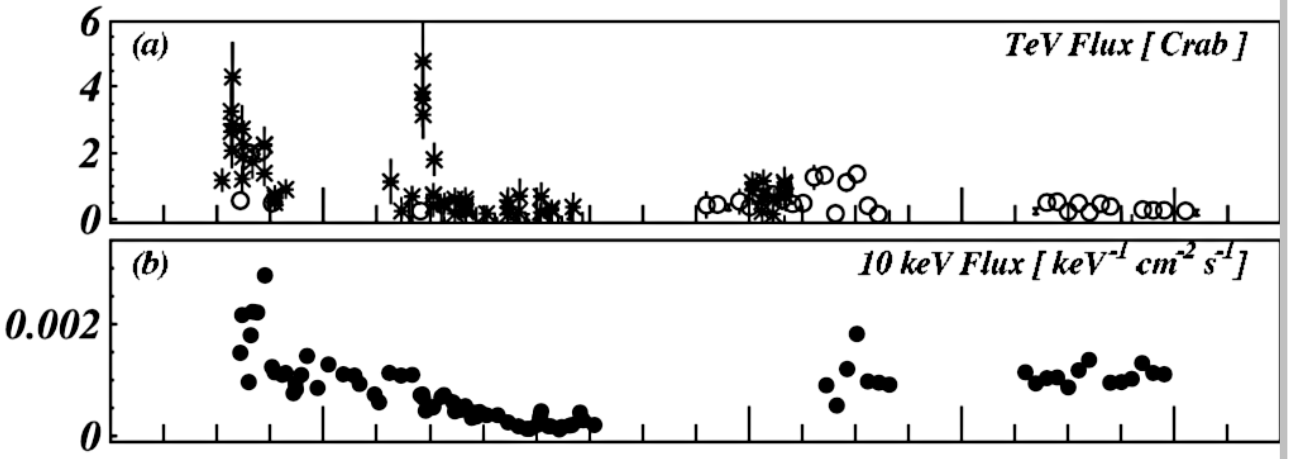

- TeV flare not not observed at other wavelengths

- some exotic models invented to describe the behavior (e.g. proton mirror model *Boettcher 2005*; similar to synchrotron mirror by *Ghisellini & Madau 1996*)

- may be produced in different regions (see A. Marscher talk yesterday)

- Klein-Nishina effects

BULK COMPTON RADIATION

- *Begelman & Sikora (1987)*: "a jet accelerated to relativistic velocities close to the black hole must Comptonize the radiation produced by accretion flow"

- jets are powered at a rate 10^{46}-10^{48} erg/s – such power has to originate deep in potential well and must be transported to parsec scales through dense radiation fields (in case of FSRQ – reprocessed UV radiation)

- cold electrons (in situ acceleration) in a steady jet produce Compton luminosity *(Sikora et al. 1997)*

$$L_{BC} \simeq 2\,\Gamma^2 \frac{1}{4} n_e r_{min} \sigma_T \xi L_{UV}$$

- which peaks at energy

$$h\nu_{BC} \simeq \Gamma^2 h\nu_{UV} \sim \left(\frac{\Gamma}{10}\right)^2 \mathrm{keV}$$

BULK COMPTON RADIATION

- using observational constraint $L_{BC}<L_{SX}$ (L_{SX} usually of the order of 10^{46} erg s^{-1}) it follows that *(Sikora & Madejski 2000)*

$$\tau \simeq \frac{n_e r \sigma_T}{\Gamma} < 0.02 \frac{L_{SX,46}}{(\xi L_{UV})_{45}} \left(\frac{\Gamma}{10} \right)^{-3}$$

so **jets must be optically very thin**

- **jets cannot be pure e^+e^- plasma** (these overproduce X-rays), **nor pure proton-electron** (but may still be dynamically dominated by protons, and loaded with pairs at larger distances)

$$\frac{n_{pairs}}{n_p} \simeq 50 \frac{L_{SX,46}}{L_{j,46}}$$

- if one additionally assumes that $L_K \sim n'_p m_p c^3 \pi r^2$, then

$$\frac{r_{min}}{r_g} > 200 \frac{n_e}{n_p} \frac{L_K}{L_{Edd}} \frac{(\xi L_{UV})_{45}}{L_{SX,46}} \left(\frac{\Gamma}{10} \right)^3$$

and **jets must form far from the black hole**

BULK COMPTON RADIATION

Celotti et al. 2007

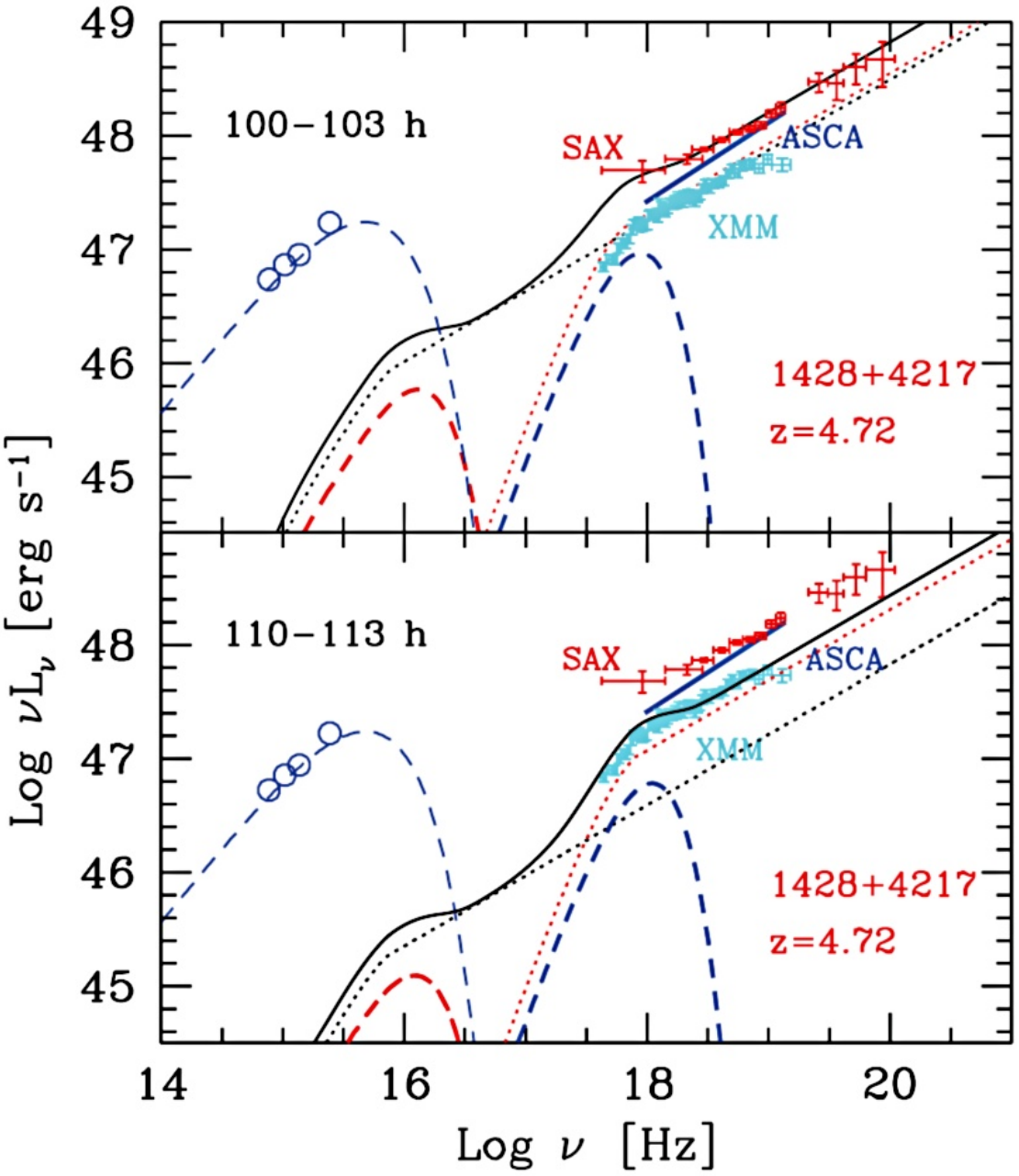

Figure 4. Illustration of how the bulk Compton process can explain some details of the X-ray spectrum of a powerful blazar,**GB B1428+4217**. The Xray data are from *BeppoSAX* (red in the online version), *XMM–Newton* (cyan in the online version) and *ASCA* (blue in the online version). The power law is assumed to start from the top of the two Comptonization humps, corresponding to the assumption that a number of leptons similar to those 'cold' are accelerated to relativistic energies and form a power-law distribution extending down to $\gamma_{min} = 1$. Top panel: spectrum predicted during 3 h of exposure time, starting 100 h after the beginning of the acceleration. Bottom panel: the same, but after 110 h. Due to the hardness of the power law, the contribution to the total power law of disc and broad-line photons is almost equal even after 100 h, despite the fact that the bulk Compton hump from disc photons is less powerful than the one from the broad-line photons. All frequencies are in the rest frame of the source.

BULK COMPTON RADIATION

Moderski et al. 2004

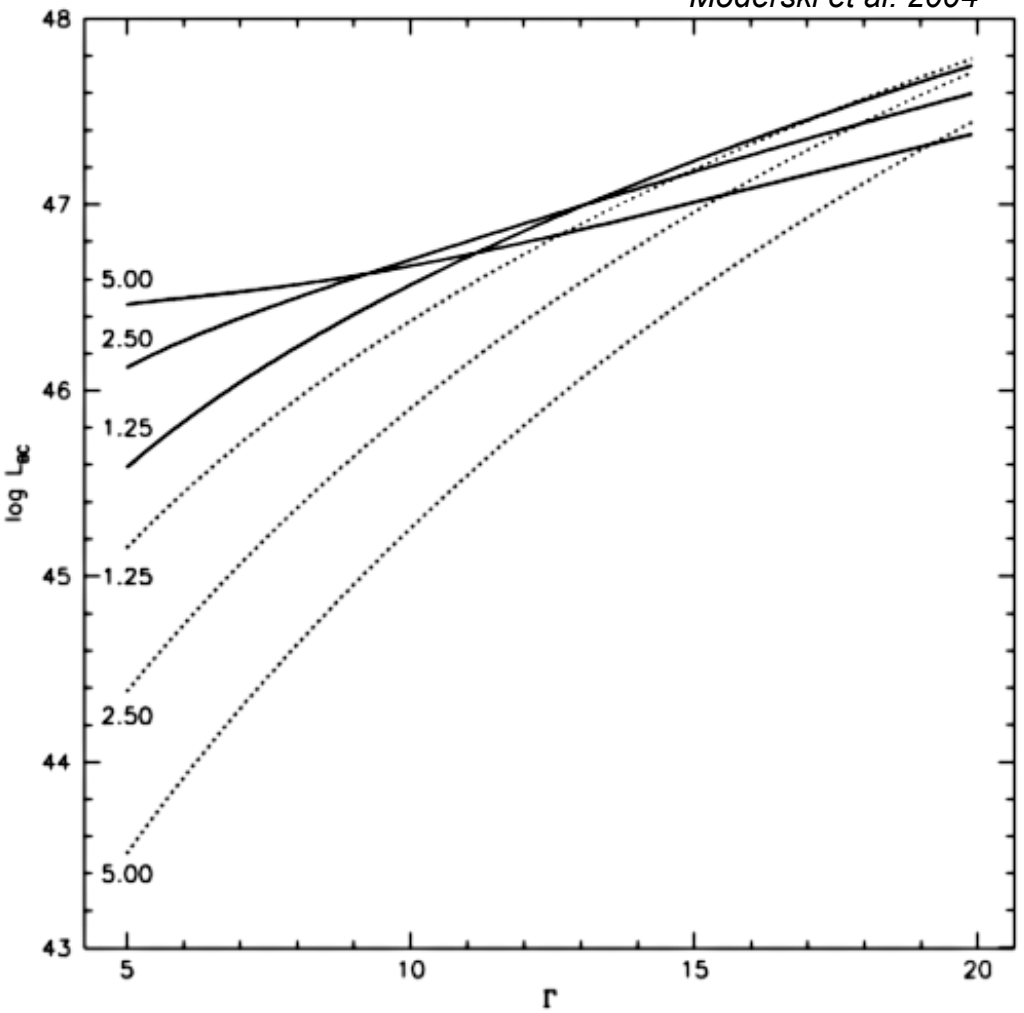

Precursor luminosity as a function of the bulk Lorentz factor. The angle of view is Θ_{obs}=1/10, and the three pairs of curves are calculated for ratio of the Lorentz factors of the two shells, α=1.25, 2.5, and 5 (marked beside the curves on the left side of the plot). The solid lines are for the faster of the two shells, and the dotted lines are for the slower of the two shells.

- internal shock model for non-thermal flares in blazars – at least **two** inhomogeneities moving down the jet with different speeds

$$L_{BC\,1,2} \simeq D^4 \frac{4}{3} c\,\sigma_T\,u_{BEL}\,\Gamma_{1,2}^2\,N_e$$

- number of electrons may be inferred from non-thermal flare

BULK COMPTON RADIATION

Kataoka et al. 2007

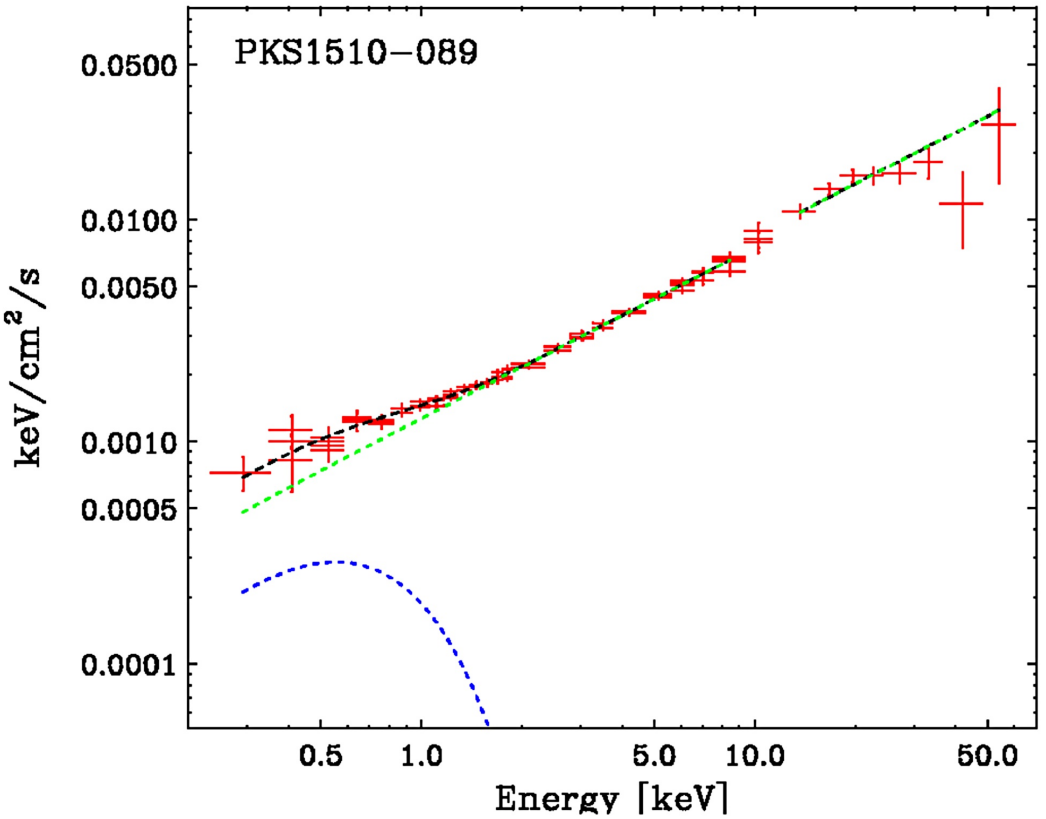

Fig. 5.— The unfolded *Suzaku* spectrum between 0.3 and 50 keV (in *vFv* space), plotted against the best-fit model composed of an absorbed power-law (Γ = 1.2: green) plus disk black body emission (kT = 0.2 keV: blue). The black line shows the sum of the model components.

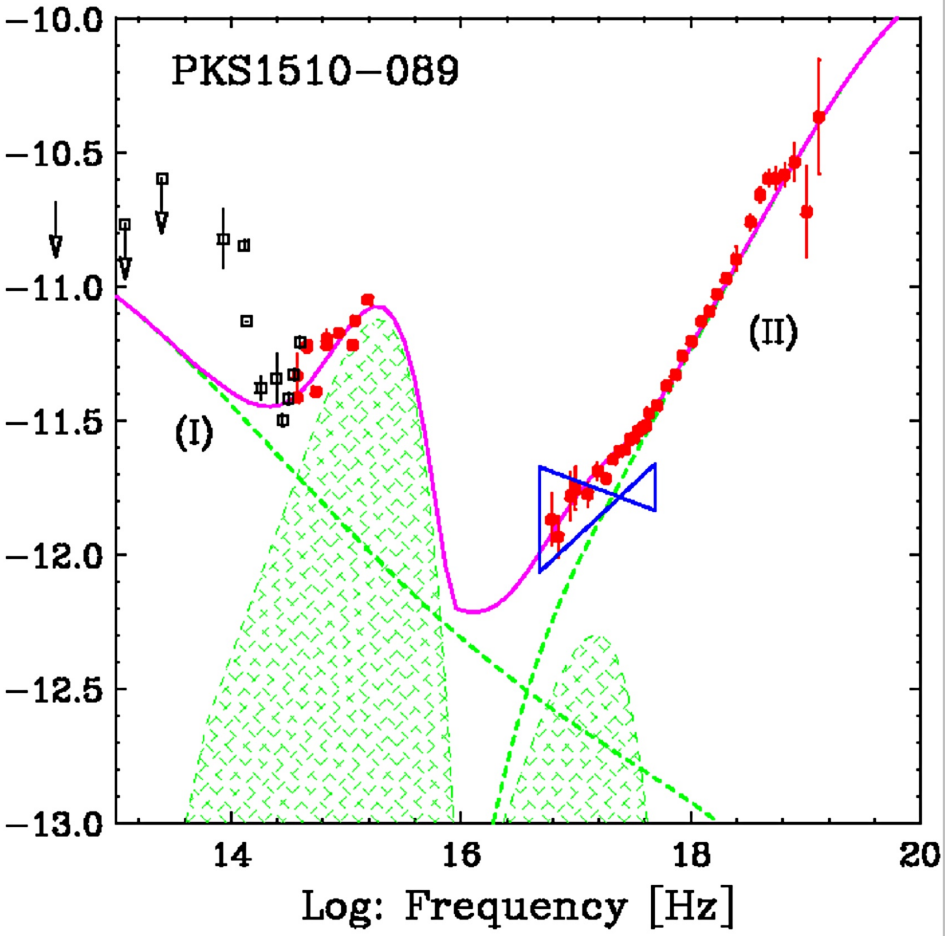

Fig. 12.— Same as Figure 11, but assuming a blackbody-type hump as predominant source to produce the soft X-ray emission. A left green hump mimics the blue bump as for Figure 11, whereas right green hump shows the best fit blackbody-type emission of *kT* 0.2 keV from the *Suzaku* fitting (Table 4). Dotted lines show (I) the Synchrotron and (II) the ERC components, respectively.

BULK COMPTON RADIATION

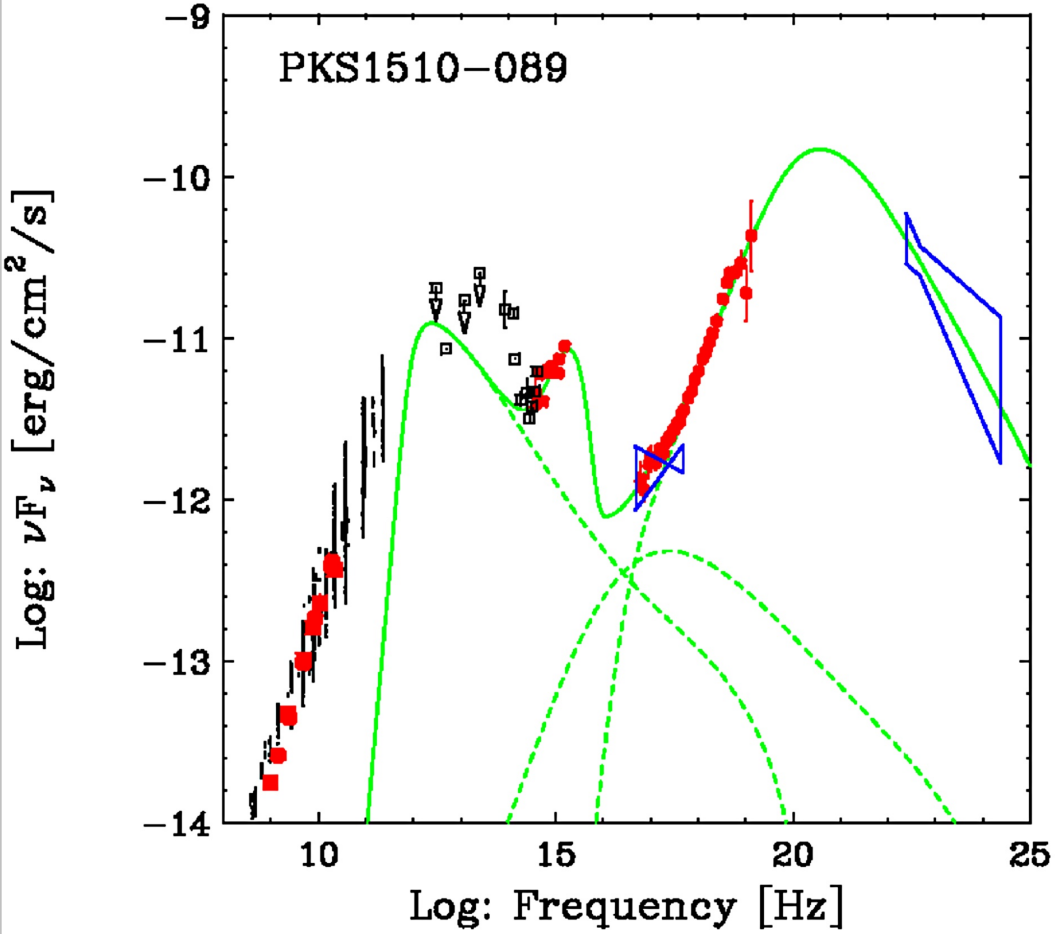

Fig. 10.— Overall SED of PKS 1510−089 constructed with multi-band data obtained during this campaign (*filled circles*): radio (RATAN-600 and ATCA), optical (*Swift* UVOT, REM and Heidelberg), X-ray (*Suzaku*). Historical data taken from radio (NED and CATS), optical (NED and Pian & Treves 1993), soft X-ray (*ROSAT*; left bow-tie from Siebert et al. 1996) and *γ*-ray EGRET; right bow-tie from Hartman et al. 1999) databases are also plotted as black points. Thick green line shows the spectrum calculated using the jet emission model, as a sum of various emission components (dotted green lines; synchrotron, SSC, and ERC; from left to right). The input parameters for this fitting are; γmin = 1, γbr = 160, γmax = 10^6, p = 1.4, q = 3.1, Ke = 1.4×10^{47} s−1, Γjet = 20, θjet = 0.02, θobs = 0.05, $r$sh = 10^{18} cm, B = 0.66Beq = 0.95 G, $r$ext = 3.0×10^{18} cm, Lext = 3.7×10^{45} erg s−1, and $h\nu$ext = 0.2 eV.

Kataoka et al. 2007

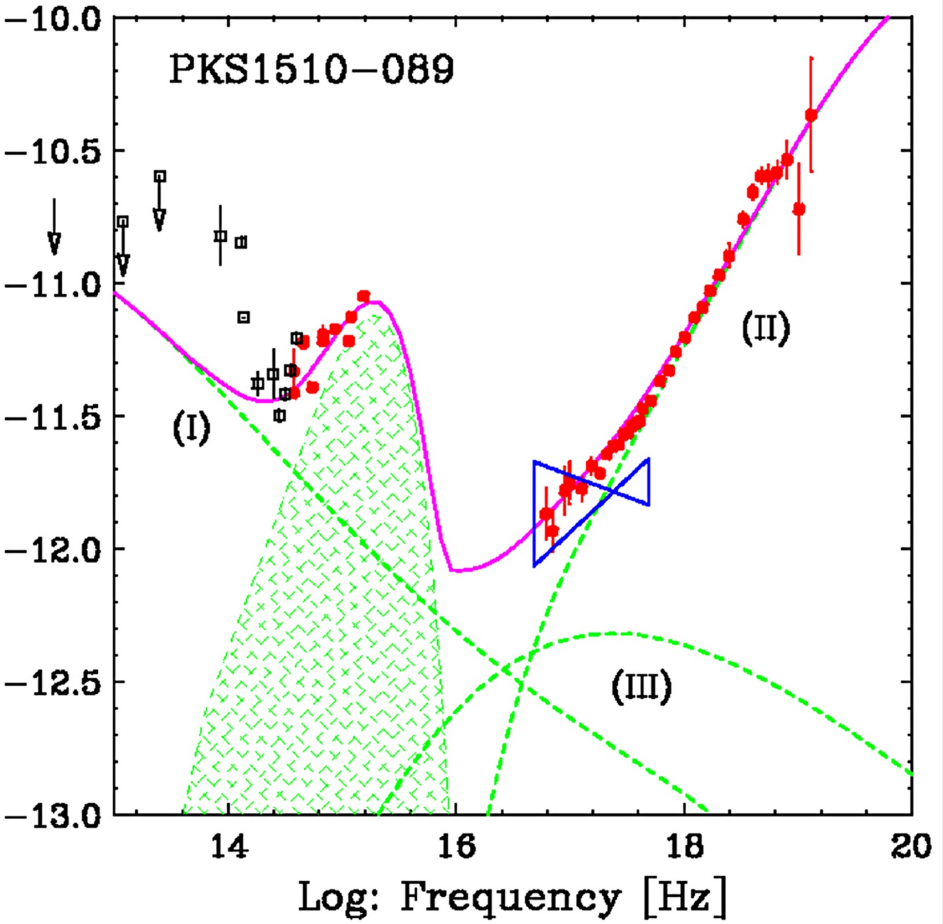

It is very difficult to distinguish BC from SSC contribution based on average spectra

BULK COMPTON RADIATION

Moderski et al. 2004

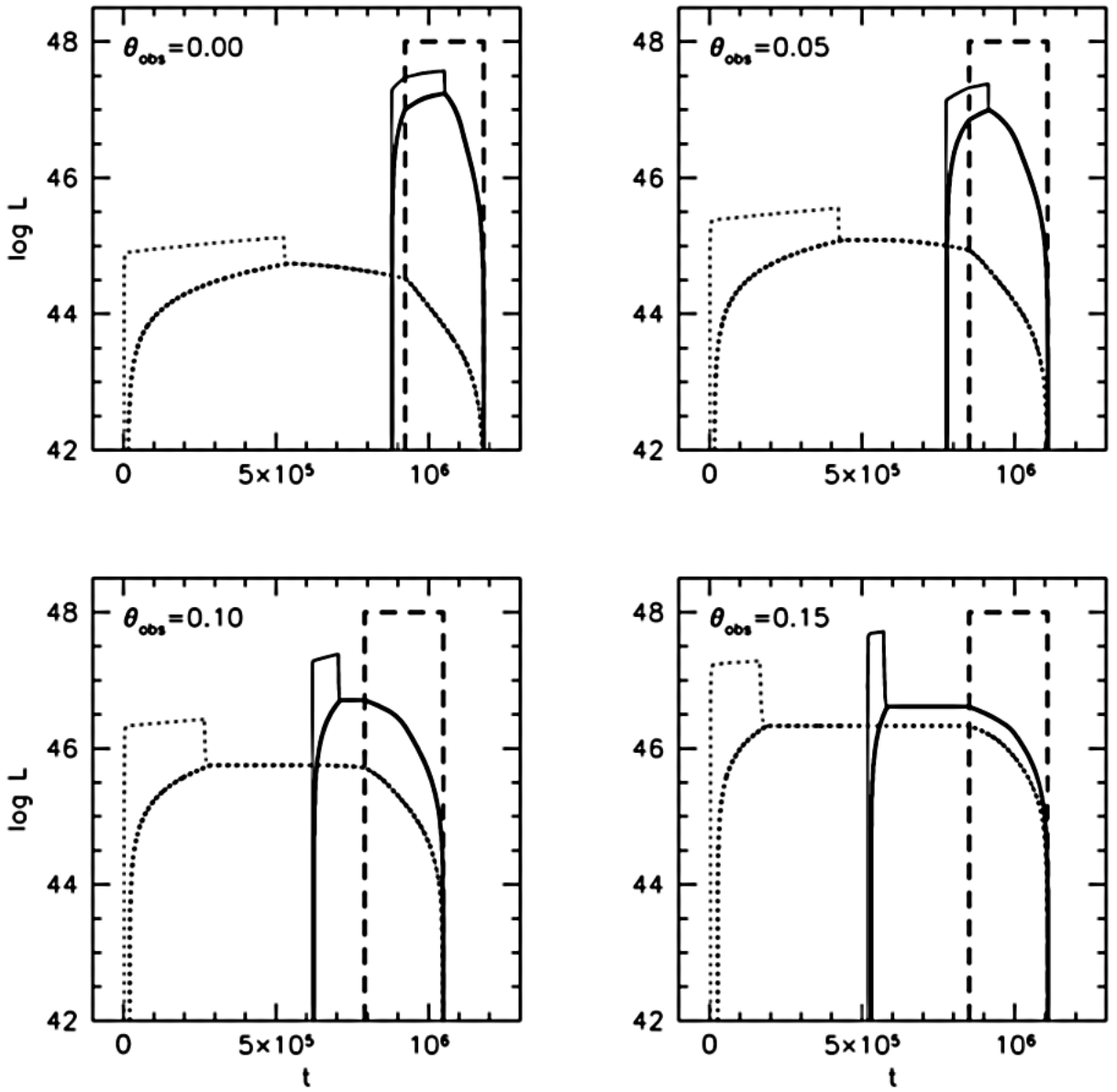

Light curves of precursors and flares for four different values of θ_{obs}. The solid lines are for the precursors produced by the faster shells, the dotted lines are for the precursors produced by the slower shells, and the dashed lines are for the non-thermal γ-ray flares as produced deeply in the fast cooling regime.

BULK COMPTON RADIATION

Moderski et al. 2004

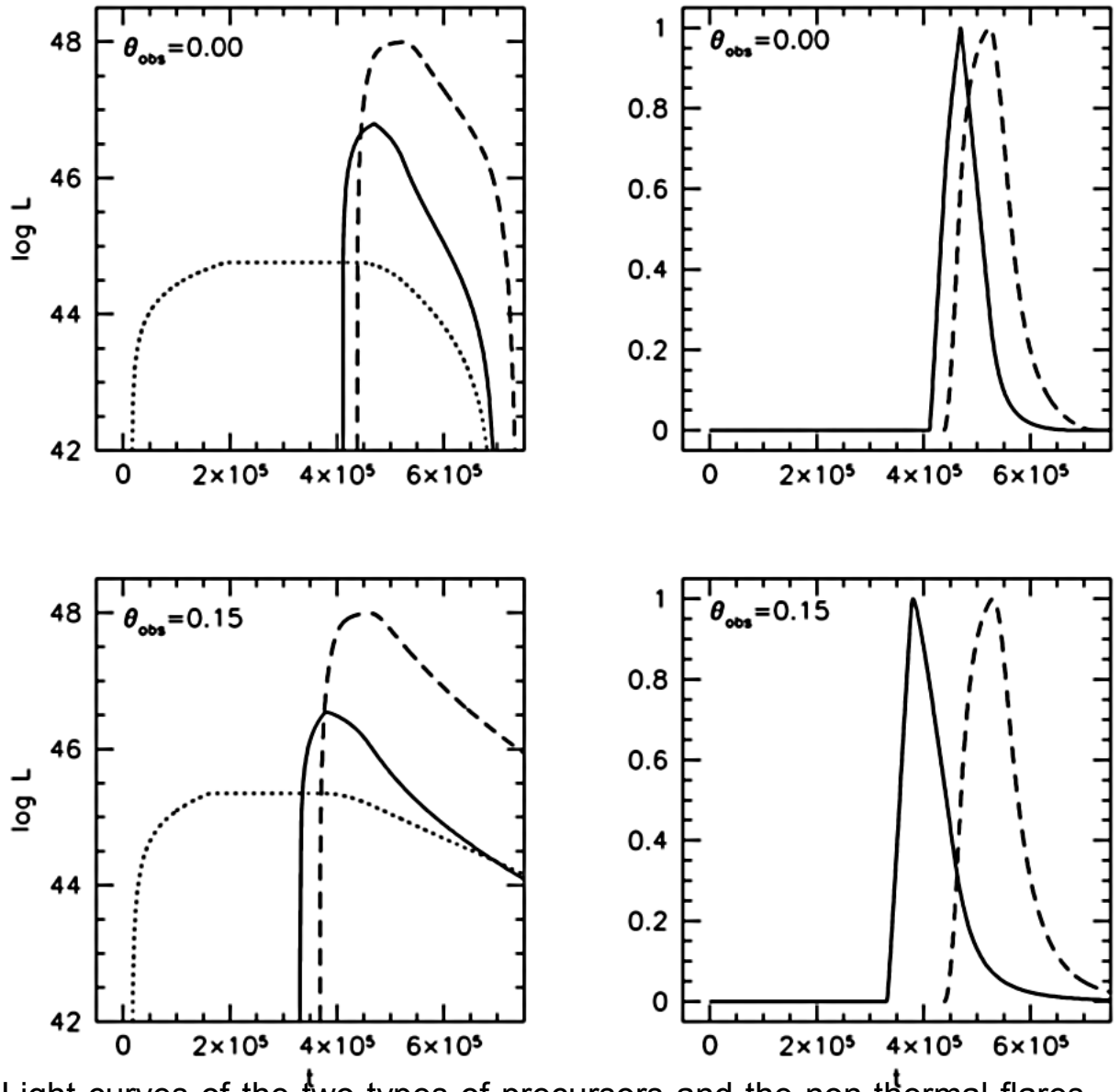

Light curves of the two types of precursors and the non-thermal flares for θ_{obs}=0 (top left) and θ_{obs}=0.15 (bottom left) for θ_j=1/Γ=0.1. Those due to the faster shells and the flares are redrawn in linear scale on the right panels with their peaks normalized to one.

- precursor from faster shell is typically 10-30 times less luminous than non-thermal flares

- this precursor should dominate the spectrum in the soft X-ray band even if SSC and EC are included

- precursor from faster shell overlaps with non-thermal flare, but decays faster (easy distinguishable from the flare)

BULK COMPTON RADIATION

- bulk Compton radiation must be taken into account in any matter dominated jet models

- currently there is no clear evidence for soft X-ray precursors (although some spectra are consistent with bulk Compton emission)

- different bulk Lorentz factors for faster and slower shells – different beaming – different temporal structure of flares (especially for off-axis observations)

- in soft X-rays situation complicated due to the Klein-Nishina effects

THE KLEIN-NISHINA EFFECTS

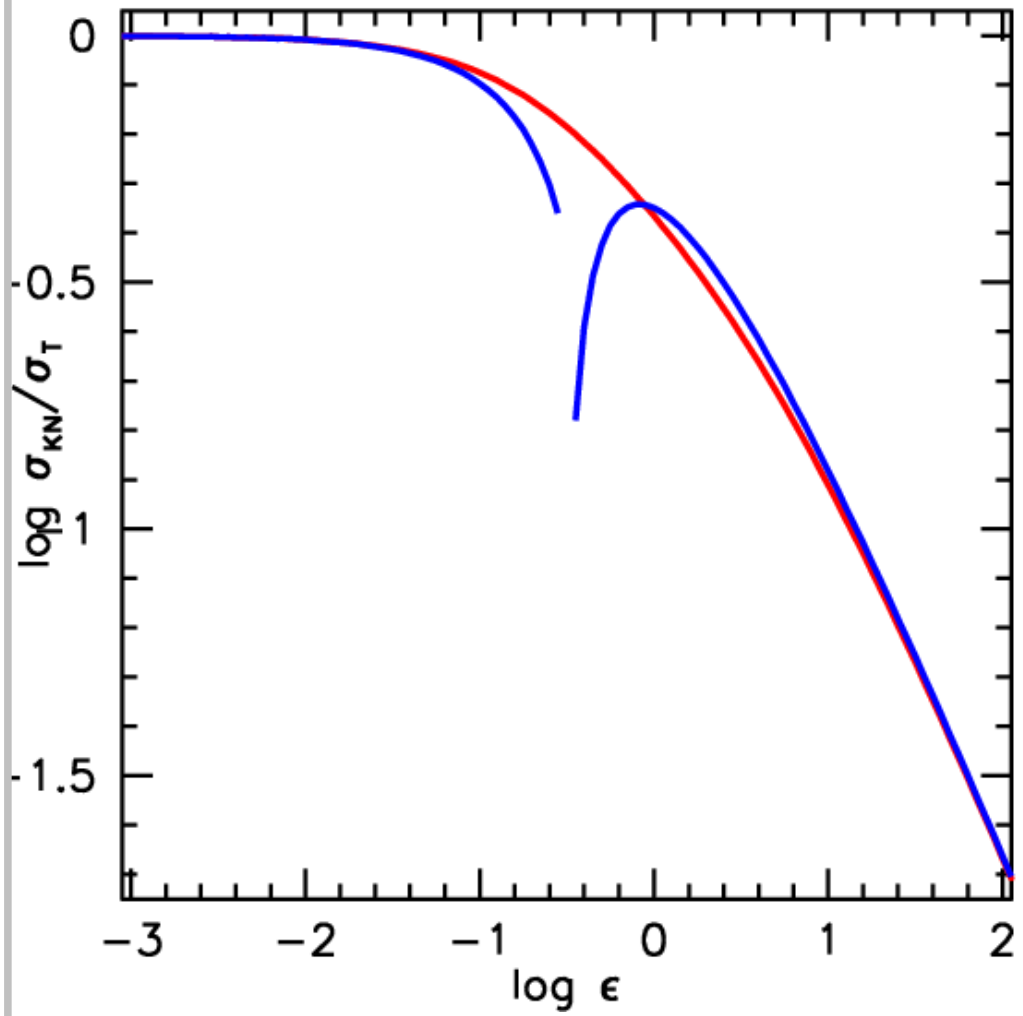

$$\gamma > \gamma_{KN} = \frac{1}{4\epsilon_0}$$

- photons cannot have more energy than $\gamma_{\max}$

$$\left(\frac{\epsilon}{\gamma}\right)_{max} = \frac{4\epsilon_0\gamma}{1+4\epsilon_0\gamma} < 1$$

- single electron can loose most of its energy in a single scattering rather than cooling quasi-continuously
- the ratio of luminosities L_C/L_{syn} is now a decreasing function of energy and is less than u_0/u_B

THE KLEIN-NISHINA EFFECTS

$$q = \frac{u_0}{u_B} \ll 1$$

- synchrotron losses always dominate over Compton losses
- steady-state electron distribution is determined by the magnetic field and acceleration mechanism
- if we assume power-law electron distribution $n_\gamma \propto \gamma^{-s}$ then:
  - the synchrotron spectrum is unchanged
  - the Compton spectrum shows a break $\Delta\alpha$ = (s+1)/2 at $\epsilon \sim \epsilon_{KN} = \gamma_{KN}$
- for sources with s>2 the break is large (>1.5) and can be misinterpreted as an cut-off due to the maximum electron energy γ_{max}

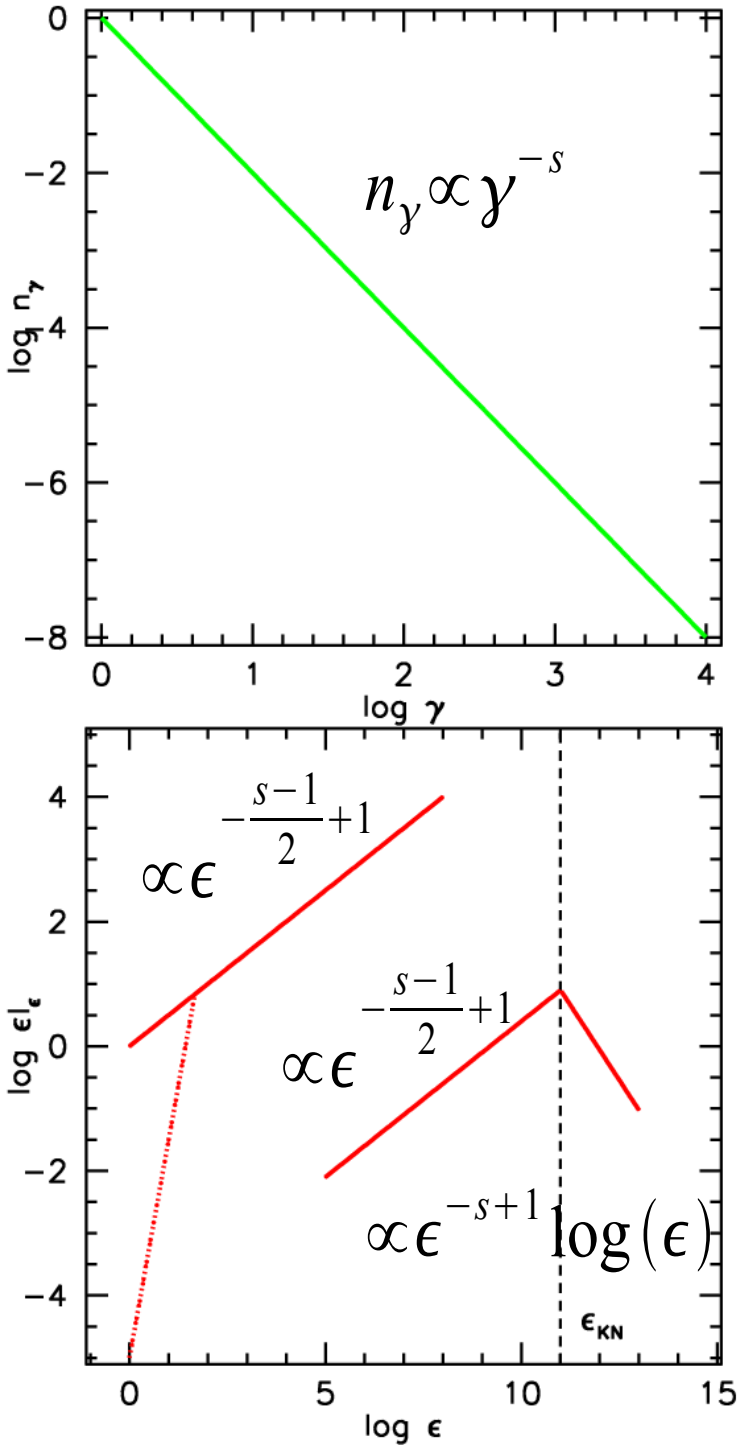

THE KLEIN-NISHINA EFFECTS

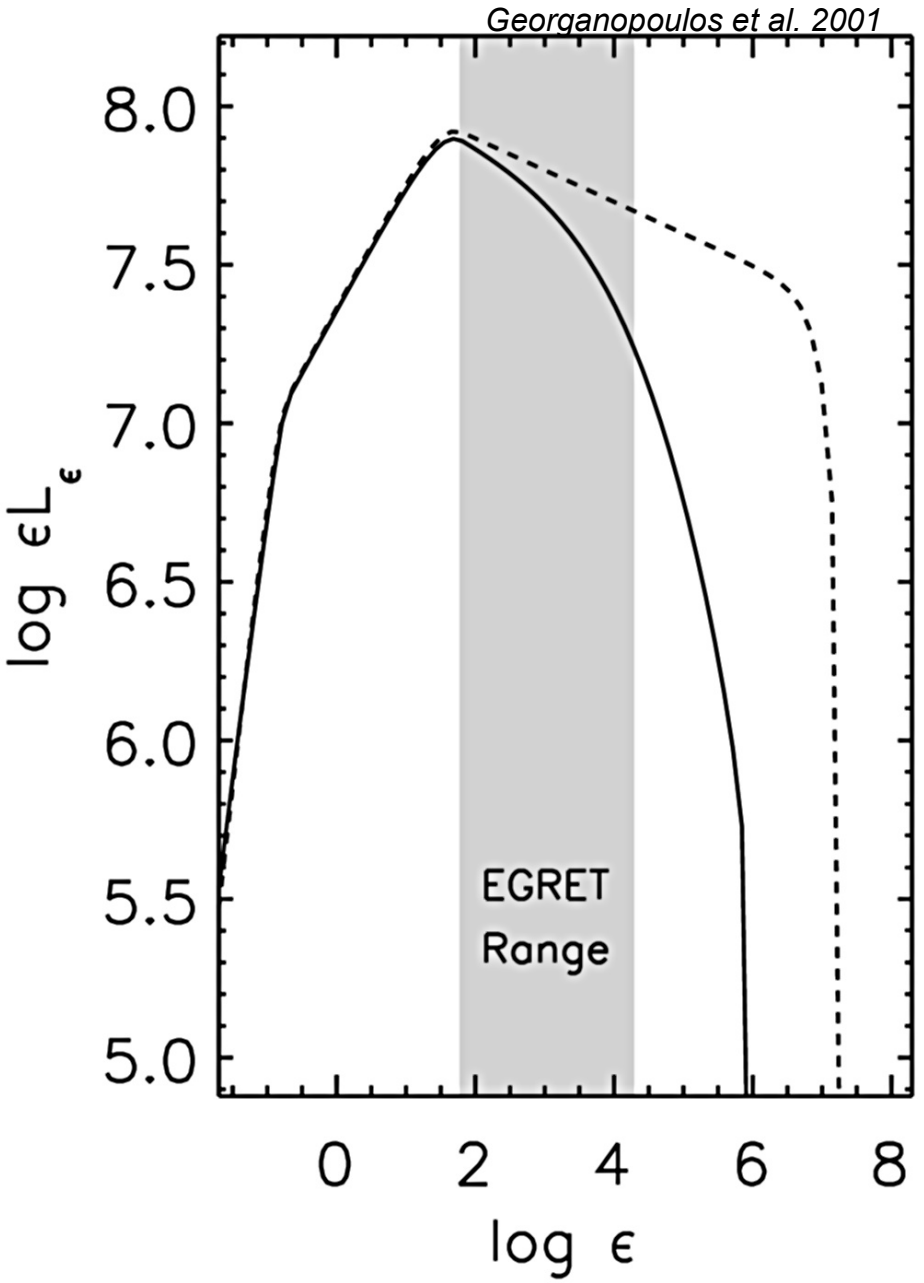

- the Klein-Nishina effects involved to explain high spectral breaks observed in MeV blazars *(Georganopoulos et al. 2001)*

but electron evolution not taken into account

FIG. 3. Observed energy distribution due to IC scattering for both the K-N (solid line) and Thomson treatment (dotted line) for a blob of plasma that moves with a Lorentz factor 10 through an isotropic mono-energetic photon field. The electrons in the blob frame are characterized by an isotropic broken power-law distribution $n(\gamma)\sim\gamma^{-p}$ with p=2.2 for $10<\gamma<2\times10^2$ and p=3.2 for $2\times10^2<\gamma<10^5$. We plot in normalized units the energy distribution due to IC scattering observed at an angle 1/Γ. The shaded area corresponds to the EGRET range of observation.

THE KLEIN-NISHINA EFFECTS

$$q = \frac{u_0}{u_B} \gg 1$$

- one can ignore the effects of synchrotron cooling (Zdziarski 1989; Zdziarski & Krolik 1993)
- steady-state electron distribution hardens for $\gamma > \gamma_{KN}$ due to less efficient electron energy losses
- this hardening compensates the decreased efficiency of Compton up-scattering, and the resulting spectrum shows no "KN break"
- the spectrum has a break at $\epsilon \sim \gamma_{max}$, independent of ϵ_0
- interesting case for p=2; $Q(\gamma) \propto \gamma^{-p}$
- for p>2 spectrum is steeper, while for p<2 harder

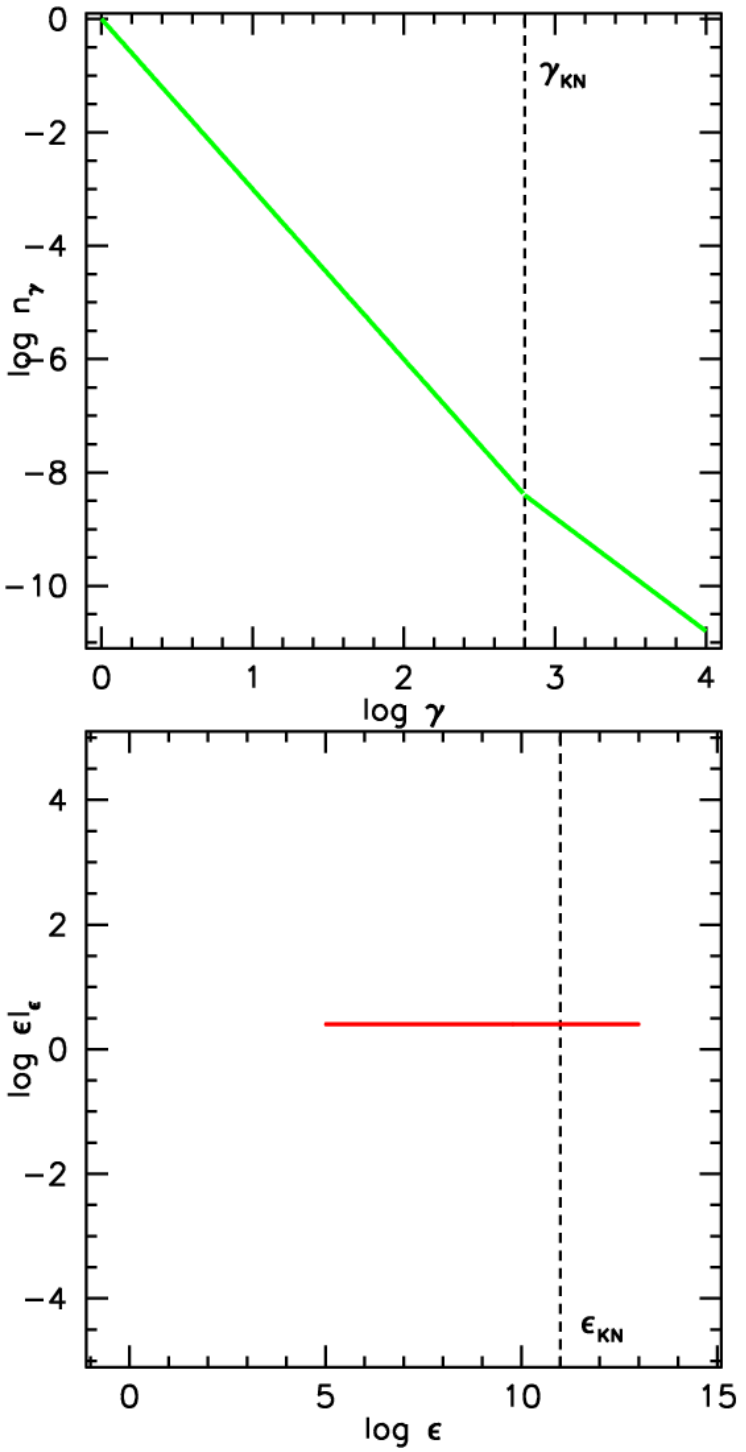

THE KLEIN-NISHINA EFFECTS

$$|\dot{\gamma}|_{IC} = \frac{4 c \sigma_T}{3 m_e c^2} u_0 \gamma^2 F_{KN}$$

$$b = 4 \gamma \epsilon_0$$

- thermal distribution of external photons is well approximated by a mono-energetic distribution with energy 2.8kT

- approximation for power law distribution of external photons

$$F_{KN} = \frac{1}{(1+b)^{1-\alpha_0}}$$

Moderski et al. 2005

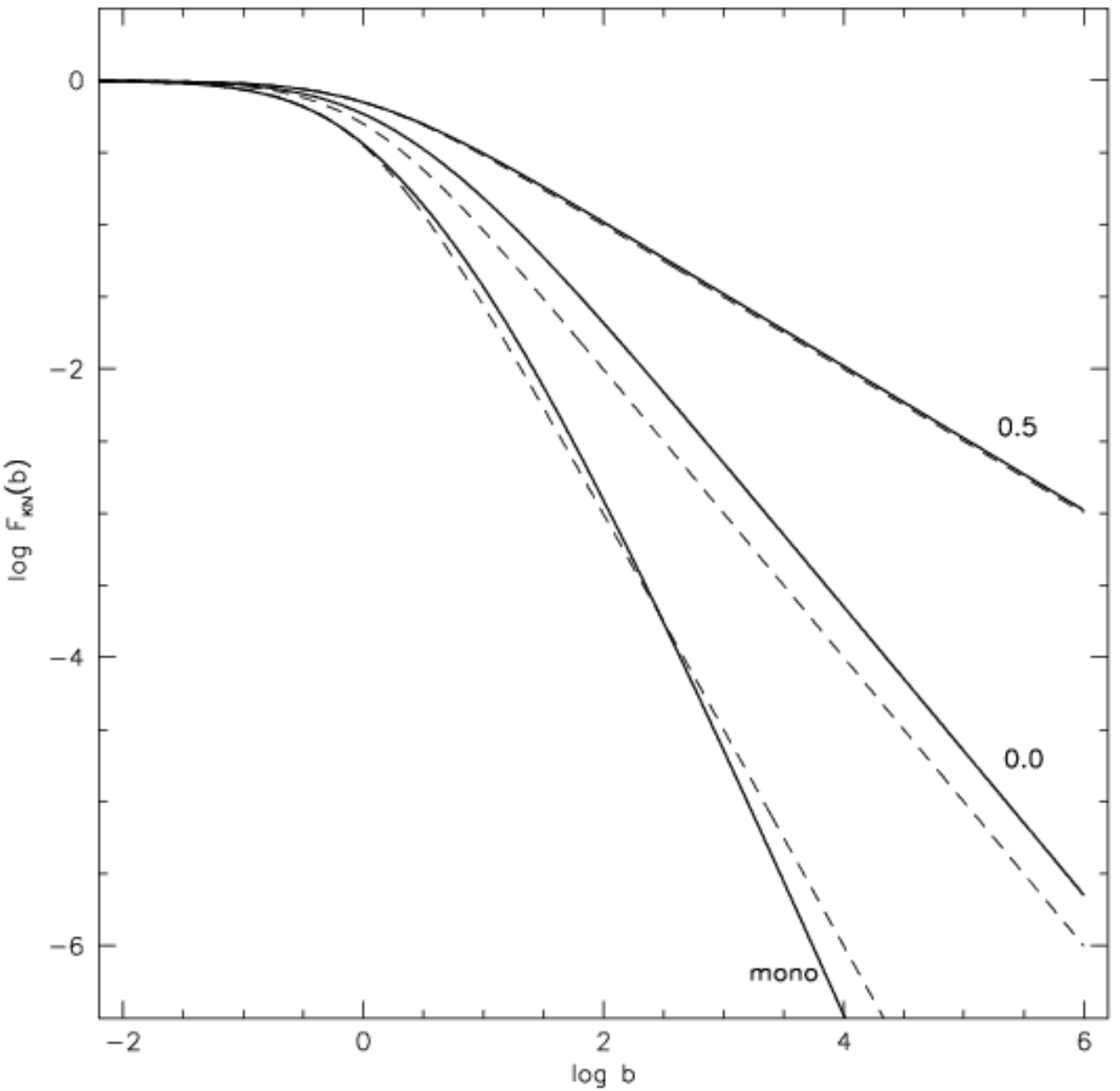

Figure 1. The function $F_{KN}(b)$ computed for mono-energetic ("mono") and power law (α_0=0.0 and α_0=0.5) energy distributions of the external photon field. The solid lines show the results of the exact calculations while the dashed lines are the analytical approximations.

THE KLEIN-NISHINA EFFECTS

$$|\dot{\gamma}|_{syn} = \frac{4\, c\, \sigma_T}{3\, m_e\, c^2} u_B\, \gamma^2 \qquad u_B = \frac{B^2}{8\pi}$$

$$\frac{\dot{\gamma}_{IC}}{\dot{\gamma}_{syn}} = q\, F_{KN}$$

- for q<1 synchrotron losses dominate for all electrons

- for q>1 there exists γ_s such that for electrons with $\gamma < \gamma_s$ IC cooling dominates while for $\gamma > \gamma_s$ synchrotron cooling dominates

For high energy electron synchrotron cooling always dominates

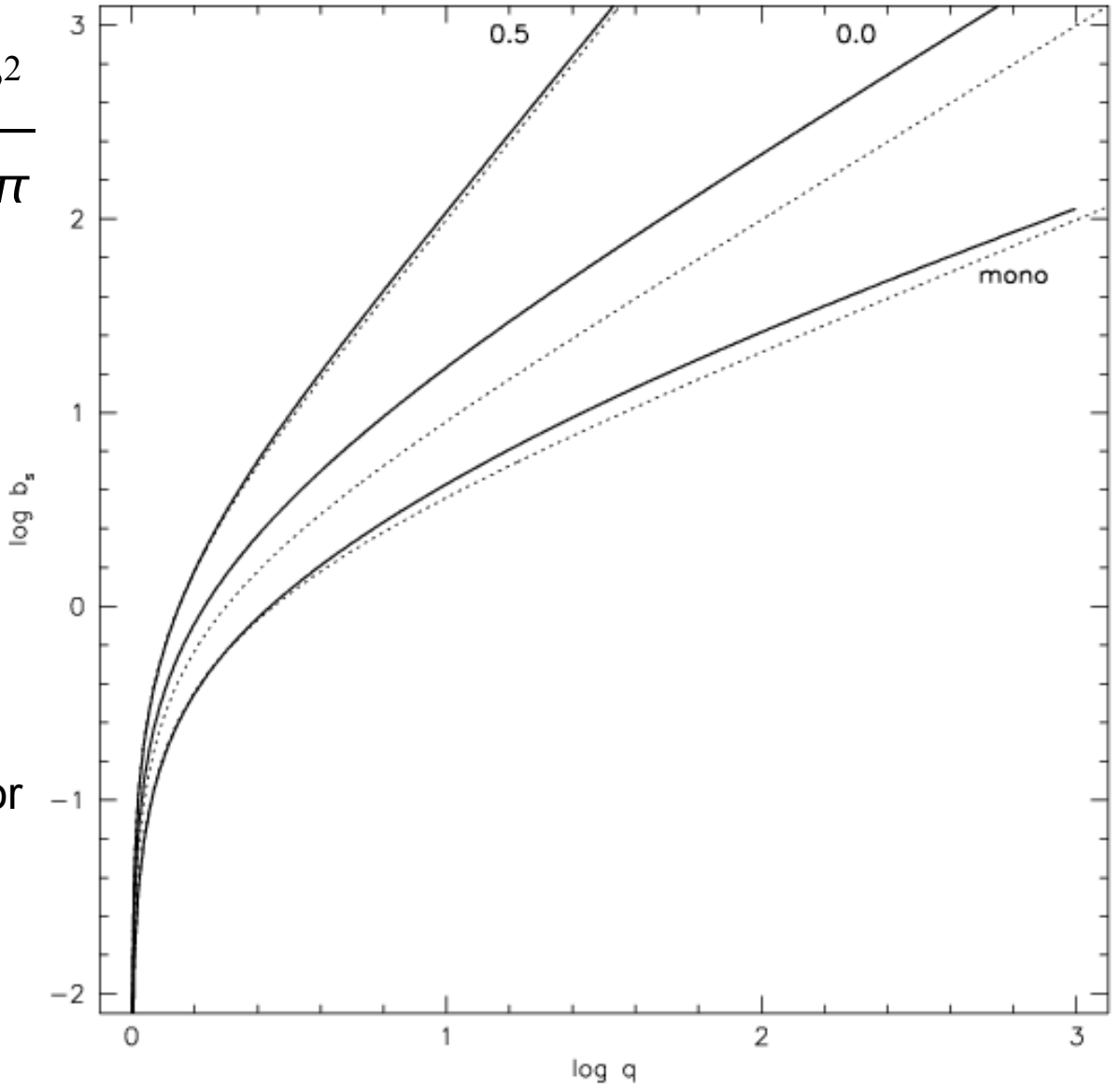

Figure 2. b_s versus q for mono-energetic and power law ambient radiation fields: solid lines, exact results; dashed lines, analytical approximations.

THE KLEIN-NISHINA EFFECTS

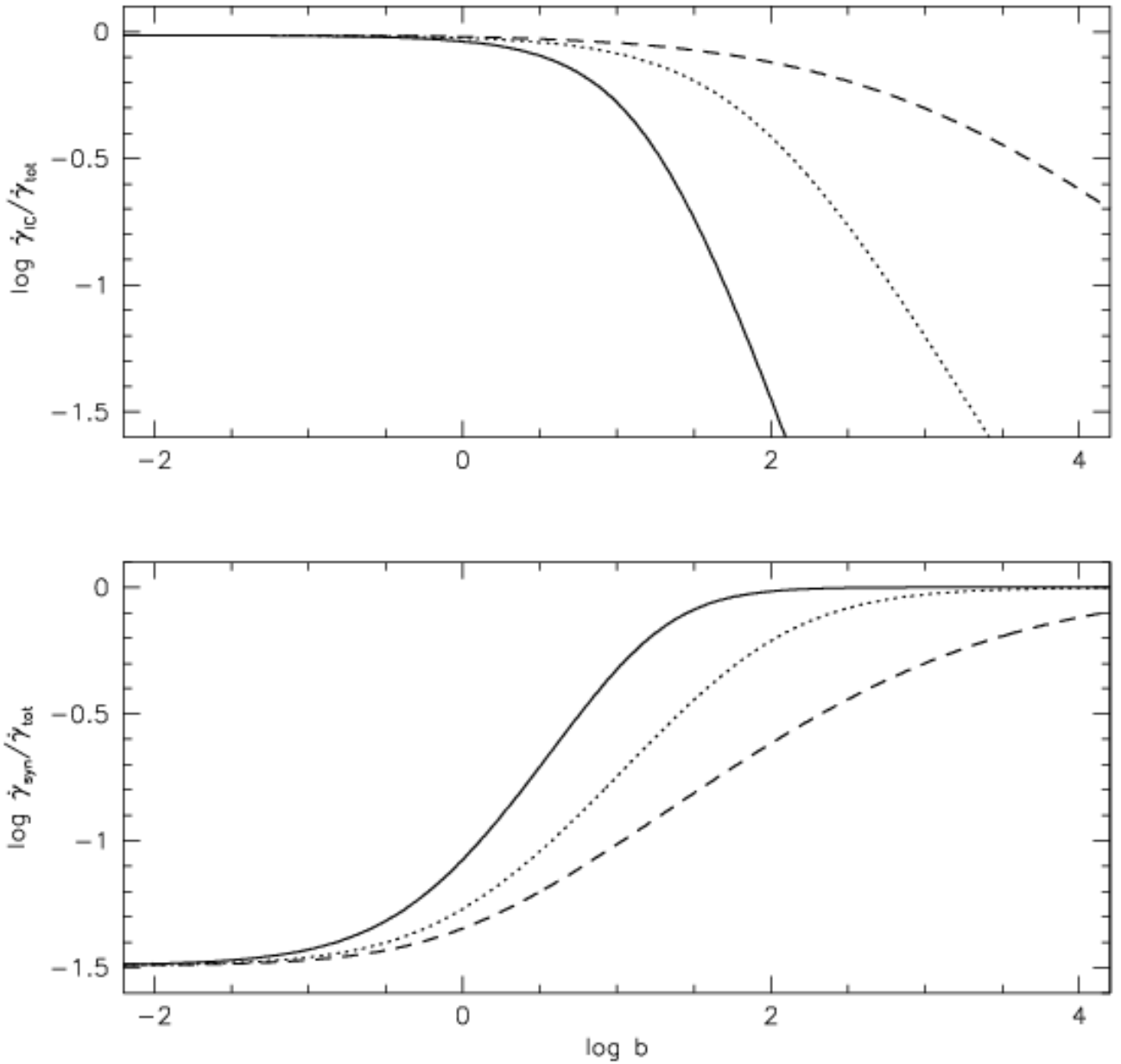

Figure 3. The relative IC and synchrotron energy losses for q=30 and an ambient radiation energy distribution that is mono-energetic (solid lines) or power law (α_0=0.0, dotted lines; α_0=0.5, dashed lines).

THE KLEIN-NISHINA EFFECTS

Steady state electron distribution

- assumptions: the acceleration is fast, electrons do not escape, no adiabatic losses

- a steady-state solution

- for $b_{max} \gg b_s$ and $q \gg 1$ the steady-state distribution has two asymptotes: one for $b \ll 1$, and one for $b_s \ll b \ll b_{max}$

- for a power-law electron injection $Q \propto \gamma^{-p}$ the asymptotes have the index s=p+1; in the middle region the electron distribution is harder

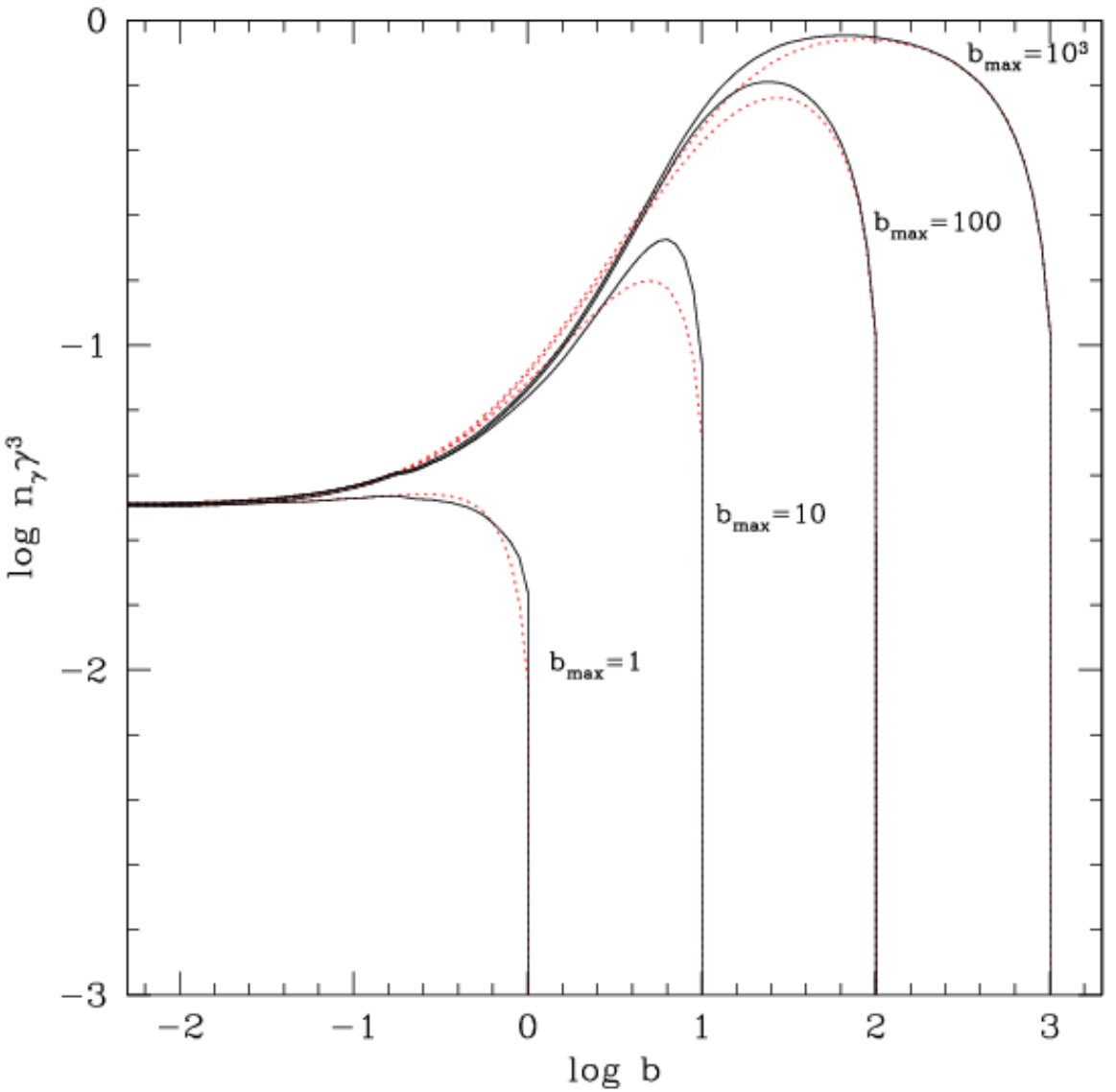

Figure 5. Steady-state electron energy distributions for the power-law electron injection function, $Q \propto \gamma^{-p}$, and mono-energetic ambient radiation field: solid lines, exact results; dotted lines, results obtained using the continuous energy loss approximation for all Compton scattering. The model parameters are: p=2, q=30, b_{max} = 1; 10; 100; 10^3.

THE KLEIN-NISHINA EFFECTS

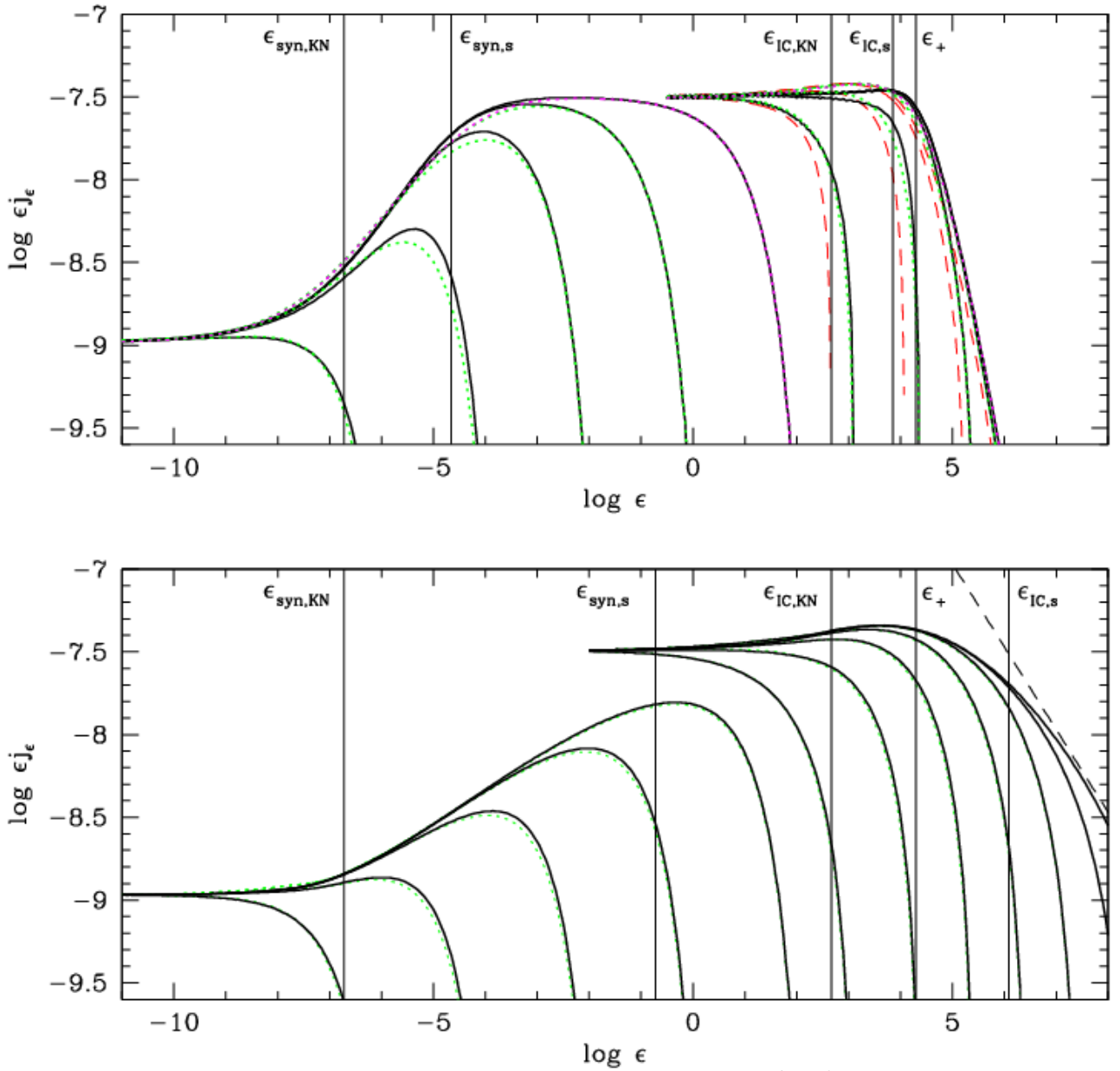

Figure 6. IC plus synchrotron spectra of steady sources with model parameters p=2; q=30; b_{max}=1, 10, 10^2, 10^3, 10^4; $\epsilon_0=10^{-4}$; B=1G. Upper panel: mono-energetic ambient radiation field. Lower panel: power-law ambient radiation field with α_0=0.5. Solid lines denote exact calculations. Dotted lines denote calculations using continuous energy loss approximation. Dashed lines denote Compton spectra computed using the continuous energy loss approximation and the delta-function approximation. The dot-dashed line in the lower panel is the asymptotic power law (α=-0.5) for the IC spectrum at $\epsilon>\epsilon_{IC,s}$.

THE KLEIN-NISHINA EFFECTS

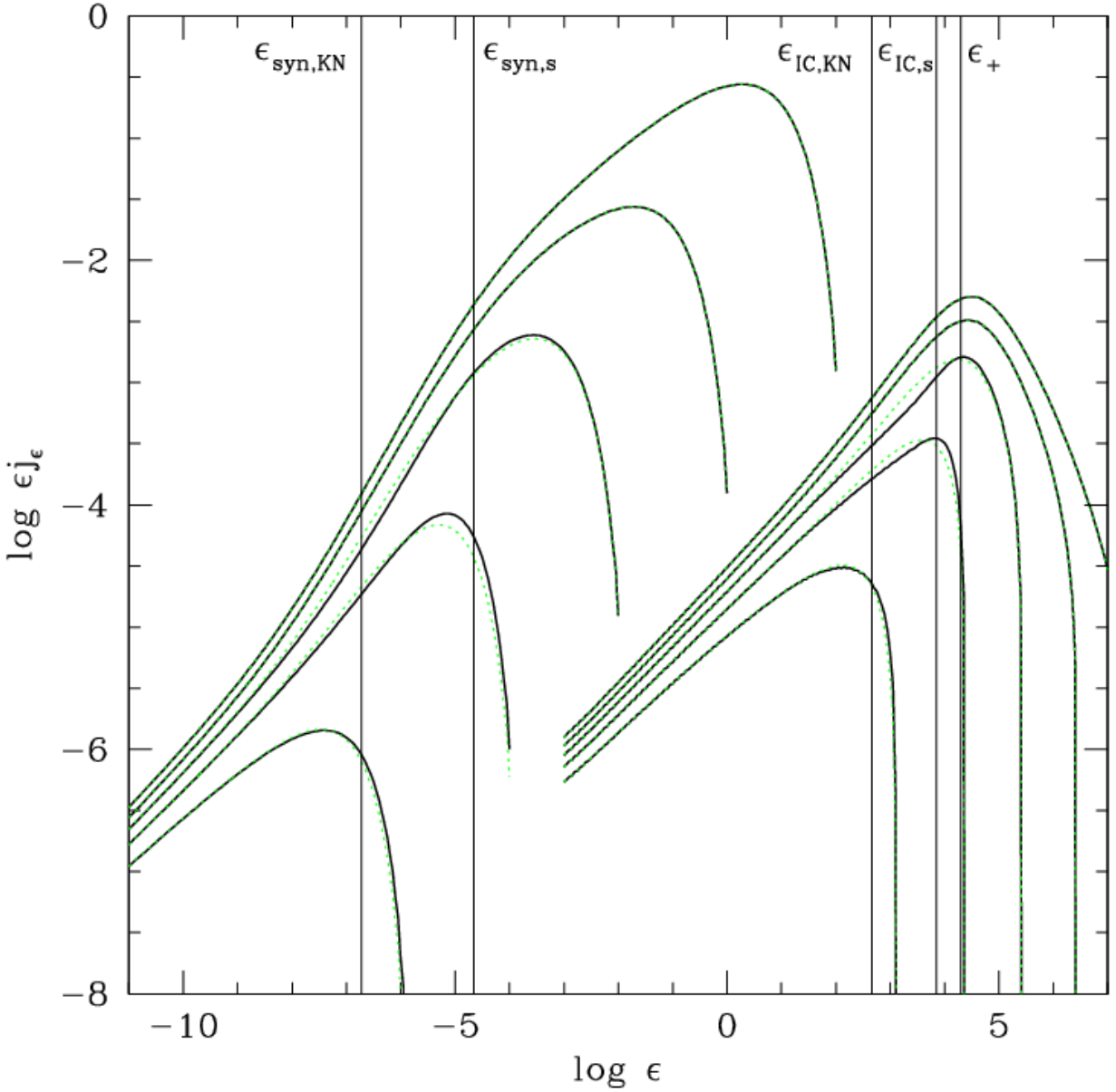

Figure 7. Same as the upper panel of Fig. 6 (mono-energetic radiation field), but for p=1.

THE KLEIN-NISHINA EFFECTS

Blazars

- flat-spectrum radio quasars are good examples of non-thermal sources with high q
- BELs are a dominant source of external radiation: $\epsilon_0 \approx 2\times10^{-5}$ (10eV)

$$\gamma_{KN} = \frac{1}{4\epsilon_0 \Gamma} \simeq 10^3 \left(\frac{\Gamma}{10}\right)^{-1}$$

$$\gamma_s = b_s \gamma_{KN} \simeq 10^4 \left(\frac{q}{30}\right)^{\frac{2}{3}} \left(\frac{\Gamma}{10}\right)^{-1}$$

$$\epsilon^{obs}_{IC,KN} \sim 1\mathrm{GeV} \qquad \epsilon^{obs}_{IC,s} \sim 30\mathrm{GeV}$$

$$\epsilon^{obs}_{syn,KN} \sim 3\times10^{13}\mathrm{Hz} \qquad \epsilon^{obs}_{syn,s} \sim 3\times10^{15}\mathrm{Hz}$$

- to show KN effects spectrum should extend beyond 1GeV; synchrotron "bump" in IR-UV
- no constraints from EGRET or TeV experiments
- for some blazars the synchrotron spectrum peaks at UV (Padovani et al. 2003) – they should have a break at 30GeV and should not be γ-ray loud

Moderski et al. 2003

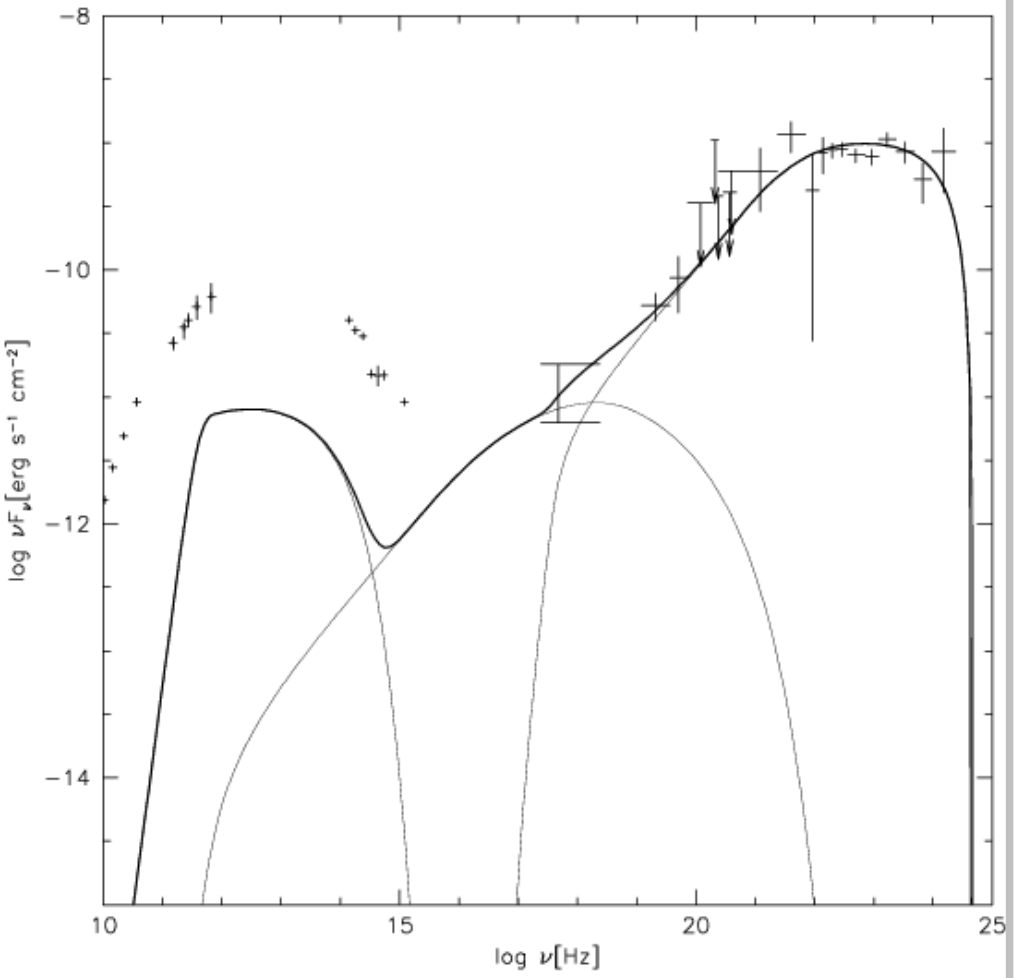

Figure 2. The average spectrum of the blazar 3C279 during the February 1996 flare. Data points are from Hartman et al. (2001). Thick, solid line shows the averaged spectrum of our model. Thin lines represent various components of the spectrum.

SUMMARY

- when studying the variability all processes of acceleration, injection, and cooling together with geometry must be taken into account – they may be responsible for a variety of observed properties from flare shapes to frequency dependent lags

- in any matter dominated relativistic jet model bulk Compton radiation may provide constraints on matter content, formation region and dynamics of the jet plasma (time dependent analysis necessary)

- Klein-Nishina effects may influence not only the high energy band, but also synchrotron component (time dependent analysis necessary)

NON-THERMAL FLARES IN BLAZARS

Double flares

Sikora et al. 2001